



Structure and sedimentation characterisation of sheared $\text{Mg}(\text{OH})_2$ suspensions flocculated with anionic polymers



Alexander P.G. Lockwood^{a,*}, Jeffrey Peakall^b, Nicholas J. Warren^a, Geoff Randall^c, Martyn Barnes^c, David Harbottle^a, Timothy N. Hunter^{a,*}

^aSchool of Chemical and Process Engineering, University of Leeds, Woodhouse Lane, Leeds LS2 9JT, UK

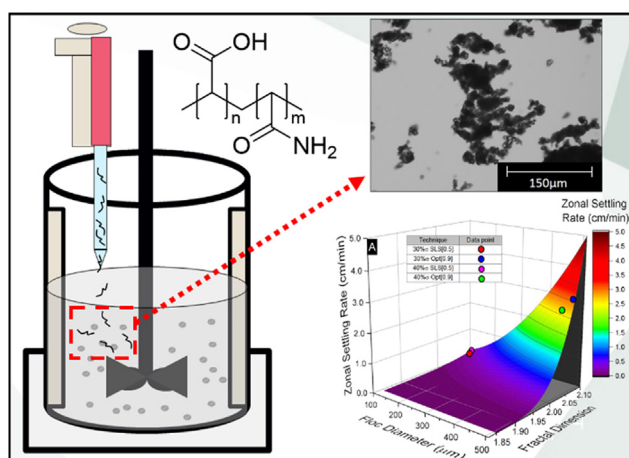
^bSchool of Earth and Environment, University of Leeds, Woodhouse Lane, Leeds LS2 9JT, UK

^cSellafield Ltd, Hinton House, Birchwood Park Ave, Birchwood, Warrington WA3 6GR, UK

HIGHLIGHTS

- Effectiveness of anionic polymers on the flocculation of $\text{Mg}(\text{OH})_2$ was established.
- Largest (d_{90}) sized flocs were more influential on the zonal settling rate.
- A Fractal Modified Richardson-Zaki predictive settling rate model was examined.
- Model provided a close first order zonal settling rate prediction, using d_{90} sizes.
- A full model sensitivity analysis highlighted fractal dimension sensitivity.

GRAPHICAL ABSTRACT



ARTICLE INFO

Article history:

Received 10 April 2020

Received in revised form 23 October 2020

Accepted 2 November 2020

Available online 8 November 2020

Keywords:

Flocculation

Anionic polymers

Extended Stokes

Sedimentation modelling

Hindered settling

ABSTRACT

In this study, magnesium hydroxide ($\text{Mg}(\text{OH})_2$) suspensions were flocculated using two polyacrylamide-poly(acrylic acid) copolymers with charge densities of 30% or 40%. Structural characteristics, including particle size distribution, shape and fractal dimension of the resultant flocs were investigated using complementary techniques; static light scattering, focused beam reflectance measurement, automated optical microscopy and cryogenic scanning electron microscopy. Sedimentation rates were analysed for 2.5 vol.% dispersions at various polymer concentrations and compared to predictions from a fractal modified Richardson-Zaki (FMRZ) settling model. FMRZ model predictions using the 90th percentile (d_{90}) floc sizes produced the most accurate correlations to experimental settling data, as these larger flocs likely dominate settling dynamics by 'netting' smaller particles. Overall, the FMRZ settling model provided a first approximation of zonal settling rates, but when further examined by multivariate analysis, was found to be critically sensitive to small changes in fractal dimension.

© 2020 The Authors. Published by Elsevier Ltd. This is an open access article under the CC BY license (<http://creativecommons.org/licenses/by/4.0/>).

* Corresponding authors.

E-mail addresses: pm12a2l@leeds.ac.uk (A.P.G. Lockwood), t.n.hunter@leeds.ac.uk (T.N. Hunter).

Nomenclature

Scripts

d	Fractal dimension [-]
D	Diameter [m]
D_f	Minimum repeating floc unit diameter [m]
D_f	Diameter of a polydisperse floc in a measured PSD [m]
D_m	Singular particle diameter [m]
D_p	Primary particle diameter [m]
d_{50}	Cumulative 50% point of diameter in a PSD [m]
d_{90}	Cumulative 90% point of diameter in a PSD [m]
F_N	Number based cumulative frequency [-]
f_N	Number based frequency distribution [-]
F_V	Volume based cumulative frequency [-]
f_s	Dimensionless permeability number [-]
f_s^*	Fractal dimensionless permeability number [-]
g	Gravitational acceleration [$m\ s^{-2}$]
$I(Q)$	Scattering intensity [-]
k	Scattering constant [-]
n	Refractive index [-]
N	Number of particles in a minimum repeating floc [-]
N_f	Number of particles in a measured polydisperse floc [-]
$P(Q)$	Single particle form factor [-]
Q	Scattering wave vector [μm^{-1}]
$S(Q)$	Interparticle structure factor [-]

U	velocity [$m\ s^{-1}$]
V	Volume [m^3]
V_f	Minimum repeating floc volume [m^3]
V_f	Measured PSD polydisperse floc volume [m^3]
V_p	Volume of a floc primary particle [m^3]
θ	Scattering angle [degrees]
λ	Wavelength of incident light [μm]
μ	Dynamic viscosity [$m^2\ s^{-1}$]
ρ	Density [$kg\ m^{-3}$]
Φ_s	Volume fraction of particles within floc [-]
ϕ	Volume fraction within whole suspension [-]
ψ	Structure prefactor [-]
ζ	Zeta potential [mV]

Subscripts

f	Floc
i	Interfacial
p	Primary particle
T	Terminal
w	Water
s	Solid particles within a floc

1. Introduction

The application of polyelectrolyte based settling agents in solid-liquid separation operations has received considerable research interest (Benn et al., 2018; Brostow et al., 2009; Franks et al., 2005; Glover et al., 2000; Heath et al., 2006; Nasser and James, 2006; Pelssers et al., 1990; Sher et al., 2013; Yan et al., 2004; Zhou and Franks, 2006). From applications in the minerals industry to water treatment and nuclear decommissioning, the reliability of suspension clarification with these additives is recognised as a low cost, simple method for optimising turbidity reduction, driving sedimentation throughput and reducing the separation process residence time (Gregory, 2009; Joseph-Soly et al., 2019). Designing gravity driven separation processes involves an in-depth understanding of the sedimentation dynamics of the system in question, particularly the role that floc structure plays in hindered settling regimes, and ultimately, which size of flocculated aggregates (or 'flocs') are most influential for determining the interfacial settling rate of these suspensions.

For example, the relationship between suspension concentration and Stokes settling rate, as originally suggested by Richardson and Zaki (1954), is often determined from the 50th percentile cumulative (d_{50}) aggregate size of the floc population. While this is a reasonable assumption if there are negligible interactions between flocs, it is known that larger flocs may encompass smaller ones into their structure as they sediment, which is an effect observed in sweeping flocculation systems (Ghernaout and Ghernaout, 2012; Jarvis et al., 2006; Shi et al., 2007). Greater influence of larger flocs on sedimentation has important implications on the nature of predictive equations, as they generally require only a single number to represent aggregate populations. Given the impact of this value in settling rate prediction, it is still largely unclear for many systems which average diameter is the most appropriate value to use in settling rate estimations (for example, 50th or 90th percentiles). Additionally, the competing effects of fractal dimension versus floc diameter on zonal settling rates requires further attention, as while denser flocs with lower effective floc volume fractions theoretically should sediment at a

greater rate, literature shows that floc size is often the dominating factor (e.g. Heath et al., 2006; Nasser and James, 2006).

It has also been suggested that fractal aggregates, whilst occupying a greater volume than non-fractal equivalents (due to more open structures of lower fractal dimension) may actually produce a vector for fluid flow through their porous microstructure reducing boundary layer separation and drag (Guan et al., 2020; Xiao et al., 2013; Heath et al., 2006; Johnson et al., 2016). Furthermore, it has been found experimentally that microflow channels exist large enough to encompass smaller agglomerates resulting in aggregate densification (Johnson et al., 2016). Additionally, given the fractal nature of flocs, the effects of the structural complexities and resultant floc density from the number and spatial distribution of particles must also be accounted for in such predictive equations. Developments in techniques such as static light scattering (Burns et al., 1997; Glover et al., 2000; Liao et al., 2005; Sorensen, 2001) have allowed for quantification of such floc characteristics, so that fractal dimension may be mathematically accounted for in predictive equations. Whilst these low volume *ex situ* sampling techniques for determining fractal dimension are advantageous for industries where large volume sampling is uneconomic or hazardous, complete removal of risk rather than mitigation is preferable. Thus, there is increasing industrial interest in the development of online or *in situ* monitoring techniques, such as focused beam reflectance meters (FBRM), to inform on floc structure and size for prediction of zonal settling rates, reducing risk to the workforce and aiding process optimisation.

Polymeric flocculation of suspended particles using charged polyelectrolytes, firstly requires the adsorption of the polymer onto the particle surface, where the mechanism is dependent on the overall charge of the polymer functional groups relative to the particle surface. In cases of like-like charge, the adsorption process is often hydrogen bonding driven, as the particle surface repels the like charged functional groups on the polymer flocculant. These interactions lead to conformational extension of the polymer chains into the aqueous medium, resulting in a number of loops and tails and the formation of large and open structures (Nasser and James, 2006). For opposing charged particle-polymer

systems, greater charge density polymers of similar chain length (with identical functionality) are expected to produce smaller, denser flocs due to their comparatively faster polymer-surface conformation kinetics with a greater fractal dimension than lower charge density counterparts (Zhou and Franks, 2006). Additionally, an increased charge density results in greater charge neutralisation, thus reducing particle-particle electrostatic repulsions and lowering adsorption free energy, which also allows denser flocs to form, as documented in previous literature (Gregory, 1988; Hogg, 2013; Nasser and James, 2006; Zhou and Franks, 2006). When considering solely the implications of fractal modified Stokes equations, higher charge density polymers are in theory expected to also dominate in hindered settling systems, due to the weighting of density and neglect of particle-particle interactions in most sedimentation models (Heath et al., 2006).

For this study, the influence of bridging polymers of varying charge density (30% and 40%) on the flocculation size, structure and sedimentation of fine magnesium hydroxide ($Mg(OH)_2$) is investigated, based on their successful use in previous work on mineral systems (e.g. Benn et al., 2018; Costine et al., 2018; Franks et al., 2005; Guérin et al., 2019; Heath et al., 2006; Hunter et al., 2020; Khelifa and Hill, 2006; Nasser and James, 2006; Sun et al., 2016). While the effect of polymer settling aids on the sedimentation dynamics of $Mg(OH)_2$ suspensions have received relatively little attention from researchers, it is an area of significant interest to the nuclear industry. In particular, large amounts of magnesium hydroxide based sludge wastes are produced from the corrosion of magnesium alloy fuel cladding, which have been stored outdoors in water cooled facilities, such as with the First Generation Magnox Storage pond, at Sellafield in the U.K. (Barlow et al., 2016; Hallam et al., 2016; Heath et al., 2018; Jackson et al., 2014). This corrosion product is required to be gravimetrically separated for ultimate containment (Maher et al., 2016). Given the expected slight cationic properties of this material's surface (Biggs et al., 2007; Johnson et al., 2016), anionic polymer settling aids are likely compatible candidates for optimising dewatering operations being undertaken (Grant et al., 2016).

To understand the polymer flocculation efficiency, several complimentary techniques are used within to fully confirm size, morphology and structural properties of the aggregates. Floc growth and shear breakdown are measured *in situ*, using focused beam reflectance measurement (FBRM) a technique utilised to investigate the kinetics of such systems in other literature (Benn et al., 2018; Cobblestick et al., 2014; Li et al., 2018; Raj et al., 2017, 2016; Vajihinejad and Soares, 2018). Static light scattering (SLS) is also used to confirm floc size and structural properties (e.g. fractal dimension) with further direct comparisons to optical microscope measurements, which have been previously applied to investigate the 2D properties of flocs in large statistical populations (>20,000) (Cao et al., 2018; Ulusoy and Kursun, 2011; Zhang et al., 2016, 2018). Complimentary cryogenic scanning electron microscopy (Cryo-SEM) is additionally performed, a technique which has allowed for an insight in polymer induced floc microstructures and internal porosity (Kim and Palomino, 2009; Krysiak-Baltyn et al., 2019; Sharma et al., 2017; Zbik et al., 2008). Importantly, the sedimentation performance of flocculated systems for various polymer doses is then measured and coupled with the obtained structural data, to evaluate the performance of settling rate predictions, utilising a fractal modified Richardson-Zaki (FMRZ) approach. Here, measured fractal dimensions are used to estimate overall floc density and volume fractions, with calculated sedimentation rates compared to those measured using d_{50} and d_{90} particulate sizes. Critically, a detailed sensitivity analysis of the settling model at a fixed $Mg(OH)_2$ concentration is also performed, which comprehensively investigates the relative influence of particle size and fractal dimension on overall predicted sedimentation rates.

2. Theory

2.1. Fractal dimension

The structural information for aggregate flocs (which are an agglomeration of two or more primary particles) are established here using SLS. In this section, the mathematical procedure to determine these values is discussed and variables defined (see also Nomenclature section). The average volume fraction of solid particles within a floc decreases as the floc grows according to Bushell et al. (2002), where the number of particles within a floc can be calculated using Eqn. (1).

$$N = \psi(D_f/D_p)^{d_f} \quad (1)$$

Here, N is the number of particles in an aggregate, ψ is the structure prefactor (a proportionality constant of order unity) which is suggested to be a function of the packing factor and the ratio of the shape factors of the aggregate and the primary particles (de Martín et al., 2014; Sorensen, 2001). D_f is the diameter of the aggregate or floc and D_p is the diameter of the primary particles (where $D_f/D_p > 1$), while d_f is the fractal dimension. It is important to note that the D_f and D_p values are determined from SLS data, which are calculated from the reciprocal microns of the wave scatter vector to determine floc structure properties (see Section 3.3) and are not representative diameters of polydisperse systems. In particular, D_f is referred to in this work as the 'minimum repeating floc size', which represents the unit cell floc structure assumed to be uniform across all flocs in the polydisperse system independent of size. Values of the prefactor, ψ , have been proposed to depend on the type of aggregation method (Tang, Greenwood and Raper, 2002), such as the relationship between ψ and d_f for $1.5 \leq d_f \leq 2.75$, as shown in Eq. (2) (Gmachowski, 1995):

$$\psi = 0.414d_f - 0.211 \quad (2)$$

The floc density, ρ_f , can be calculated from the average volume fraction of the solid particles in the floc, Φ_s , the average volume fraction of water in the floc being the porosity, $1 - \Phi_s$, and the solid and liquid densities (ρ_p and ρ_w) as per Eqn. (3) (Bushell et al., 2002):

$$\rho_f = \Phi_s \rho_p + (1 - \Phi_s) \rho_w \quad (3)$$

The density of the floc, ρ_f , can then be evaluated in terms of particle number per floc and volume of components as displayed in Eq. (4):

$$\rho_f = \frac{(NV_p \rho_p) + (V_f - NV_p) \rho_w}{V_f} \quad (4)$$

Here, V_p is the volume of the primary particles (thus NV_p is the total volume of solid components in a floc) and V_f is the volume of the minimum repeating floc diameter D_f , including the internal trapped liquid (Tang et al., 2002).

2.2. Modified Stokes law

Floc settling rates for suspensions of intermediate concentration have been widely investigated (Font and Pérez, 2000; Johnson et al., 2016; Kinoshita et al., 2017; Nasser and James, 2009; Wu and Adachi, 2016). As particles settle, they displace fluid below them in a batch settling regime, where this fluid displacement may hinder settling in the system. Thus, the Stokes law of terminal settling velocity may be modified by Eq. (5):

$$U_i = U_T \times f_s \quad (5)$$

The terminal velocity of an individual particulate, U_T , is calculated using Stokes law which determines the terminal settling velocity of a singular particle of diameter, D_m . Whereas the velocity of the sediment interface (or zonal settling front) in hindered settling systems, U_i , is determined as a product of a dimensionless function proportional to the permeability of the particle network suspended in the medium (referred to here as the dimensionless permeability number, f_s), and the individual particulate sedimentation velocity under terminal conditions, U_T , as displayed in Eq. (6), where additionally 'g' is acceleration due to gravity and μ_w is the viscosity of water.

$$U_i = \frac{g(\rho_p - \rho_w)D_m^2}{18\mu_w} f_s \quad (6)$$

Adachi and Tanaka (1997) and Adelman et al. (2013) used a modified terminal settling rate equation that incorporated the fractal nature of the settling flocs shown in Eq. (7):

$$U_i = \frac{g(\rho_p - \rho_w)\bar{D}_f^2}{18\mu_w} \left(\frac{D_f}{D_p}\right)^{d_f-3} f_s^* \quad (7)$$

where \bar{D}_f represents the value of a floc diameter selected to represent the polydisperse floc population (i.e. d_{50} or d_{90}) which is measured by SLS, FBRM and optical microscopy and determined from their respective particle size distributions (PSDs). f_s^* is the fractal modified dimensionless permeability number (see explanation below). Richardson and Zaki (1954) suggested the following relationship in Eq. (8), for multiple spherical particles settling in laminar flow conditions, stating that the traditional particle dimensionless permeability number of the suspended medium, f_s , is a function of the particulate volume fraction and an exponent, which is traditionally also a function of Reynolds number (Camenen and Pham Van Bang, 2011; Johnson et al., 2016) and normally taken as equal to 4.65 in laminar conditions.

$$f_s = (1 - \phi_p)^{4.65} \quad (8)$$

Here ϕ_p is the volume fraction of the settling particle species in dispersion (as opposed the fraction of particles in a floc, Φ_s). While originally determined for discrete objects, the hindered settling model has been expanded, as originally described by Michaels and Bolger (1962) and a number of proceeding authors (Heath et al., 2006; Khelifa and Hill, 2006; Meakin, 1988; Johnson et al., 2016) to account for the effective fractal volume fraction of aggregate flocs, with respect to the dispersed particles. This modification is given Eq. (9), where ϕ_f is the effective volume fraction of the aggregate flocs.

$$\phi_f = \phi_p \left(\frac{D_f}{D_p}\right)^{3-d_f} \quad (9)$$

Finally, Eqs. (7)–(9) can be combined (substituting ϕ_f for ϕ_p to derive the fractal modified dimensionless permeability number f_s^*) giving an overall Fractal Modified Richardson-Zaki model (referred to as the FMRZ model from hereon), as used by Heath et al. (2006) and Hunter et al. (2020), in Eq. (10):

$$U_i = \frac{g(\rho_p - \rho_w)\bar{D}_f^2}{18\mu_w} \left(\frac{D_f}{D_p}\right)^{d_f-3} \left(1 - \phi_p \left(\frac{D_f}{D_p}\right)^{3-d_f}\right)^{4.65} \quad (10)$$

3. Materials and methodology

3.1. Materials

Versamag Mg(OH)₂ (Martin Marietta, US) was used for all experiments. Versamag is a fine, white precipitated powder with

a solubility of 6.9 mg l⁻¹ at pH 10.1 in water (Martin Marietta Magnesia Specialties, 2016). Initial characterisation of the dry and suspended Mg(OH)₂ was completed to understand the non-flocculated size and morphology. Detailed methodology is provided within the Electronic Supplementary Material (ESM) including a scanning electron micrograph of the dry Mg(OH)₂ and energy dispersive X-ray (EDX) analysis of Mg(OH)₂ in ESM Figs. S1 and S2 respectively. The 50th percentile cumulative particle size, zeta potential, Brunauer–Emmett–Teller (BET) surface area, bulk suspension pH and average fractal dimension (see SLS data in ESM Fig. S3) are provided in Table 1. It is noted that the high equilibrium pH is due to the self-buffering nature of magnesium hydroxide because of its partial solubility. The powder is present as particles of fused nanocrystallite platelets, as described previously (Johnson et al., 2016) which gives rise to the large relative surface area in terms of that expected from spherical equivalent estimations (Elliott et al., 2018). Thus, there are many potential interaction sites with the charged anionic polymers for a given volume fraction, although the low magnitude of the zeta potential may reduce the interaction strength. A fractal dimension of 1.97 suggests that the raw Mg(OH)₂ aggregate via a ballistic cluster-cluster aggregation mechanism (de Martín et al., 2014).

The polymers used in the study were water soluble anionic polyacrylamide-poly(acrylic acid) copolymers, AN934SH and AN945SH (SNF® Ltd) of similar molecular weight (approximately 1.4 × 10⁶ g mol⁻¹, as provided by the supplier) with charge group densities of 30% and 40% respectively. 1 g of the powders provided were dissolved in 1 l deionised water batches to produce stock polymer solutions of 1000 ppm that could be sampled and diluted accordingly. In this work, the polymers AN934SH and AN945SH will be referred to as '30%σ' and '40%σ' respectively, as a reference to their charge density.

3.2. Production of flocculated particle suspensions

Two suspension-polymer systems were characterised using various analytical techniques, where the Mg(OH)₂ particle concentration was set at 2.5 vol% in all cases, to reflect the typical particle loading of sludge transfers from legacy nuclear waste spent fuel ponds (Grant et al., 2016; Hunter et al., 2020). Added 30%σ and 40%σ polymer dosages were varied, ranging from 5 ppm to 20 ppm (mg of polymer per litre of suspension) as these dosages are consistent with much literature on the flocculation of minerals using similar charge density polymers (Benn et al., 2018; Heath et al., 2006; Nasser and James, 2006). In particular, the same polymers have been used successfully to flocculate calcium carbonate suspensions (Hunter et al., 2020), which have similar size distributions and surface charge (Elliott et al., 2018). Flocculated suspensions were prepared in a 1 l reactor vessel, 25 cm in diameter with four baffles and mixed using a four-blade axial flow impeller of 50 mm diameter, and 60° pitch, which was located 2 cm from the base of the reactor vessel. Impeller rotation rate was at 300 rpm, as this was determined to be a sufficient agitation rate to keep flocs suspended and prevent sedimentation, while reducing shear degradation experienced with higher mixing rates. The required polymer was then added in 5 ml aliquots via a calibrated micropipette over a period of no more than 10 s at the centre of the suspension, to ensure an even distribution throughout the system.

For determination of reactor vessel residence time, a study of the *in situ* floc growth kinetics was conducted using a Lasentec® Focused Beam Reflectance Measurement (FBRM) model PI-14/206 instrument (Mettler-Toledo) in macro mode. The reactor was set-up with the FBRM probe mounted at a 45° angle to the impeller shaft and 10 cm from the reactor vessel base within the mixing zone, to ensure representative flow of suspended particles past the measurement window (Barrett and Glennon, 2002). A sche-

Table 1Physical characteristics of Mg(OH)₂ suspensions; median particle diameter (d_{50}), zeta potential, surface area and equilibrium pH.

d_{50} (μm)	ζ -Potential (mV)	BET Surface Area (m^2g^{-1})	pH	Fractal dimension [d_f]
~2.5	~12	~8	~10.1	1.97

matic of the mixing reactor with inserted FBRM is given within the ESM (Fig. S4). The chord length distribution (CLD) of the system was monitored by taking measurements every 5 s for 1 h, and subsequently processed to produce a number percentage based d_{50} chord length with time. Chord length number distributions were then computationally translated to volume percentage spherical equivalent diameters, assuming floc sphericity, as outlined by Rhodes (2008) similar to techniques used by Li and Wilkinson (Li and Wilkinson, 2005). For a number based cumulative frequency distribution as function of floc diameter, F_N , and corresponding frequency distribution f_N (or $\frac{dF_N}{dD_f}$), conversion to a volume based cumulative frequency distribution (F_V) can be computed by the relationship suggested by Rhodes (2008) shown in Eq. (11). Therefore, the cumulative volume based distribution of flocs obtained from FBRM analysis can be determined from the number based distribution using Eq. (11) (Rhodes, 2008). These data were then used to determine a suitable reactor residence time to produce stable flocs for sedimentation performance and structural characterisation.

$$F_V = \frac{\int_0^{\bar{D}_f} \bar{D}_f^3 f_N d\bar{D}_f}{\int_0^{\infty} \bar{D}_f^3 f_N d\bar{D}_f} \quad (11)$$

3.3. Size and structural characterisation

Static light scattering (SLS) was used to measure both the size distributions of the flocculated suspensions and determine their fractal dimension. Here, 1 l suspensions of Mg(OH)₂ were flocculated with 20 ppm of 30% σ and 40% σ polymer for 1000 s, as described in Section 3.2. The suspension was then transferred to a 1 l measuring cylinder and inverted 5 times to meet the shear conditions in the sedimentation tests (detailed below). A 5 ml aliquot was then drawn from the measuring cylinder and added to a Mastersizer 2000E (Malvern Panalytical Ltd) using a Hydro 2000SM aqueous dispersion cell (external dimensions of 140 × 175 × 390 mm and sample volumes between 50 and 120 ml). The dispersion unit was pre-filled with 120 ml of deionized water dosed with a polymer solution background, providing a polymer concentration gradient to prevent desorption of polymer from the particle surface. Importantly, the unit was sheared at 900 rpm to ensure consistent flow of suspensions through the vertical optical window and to prevent particle deposition, meaning that there was some potential for additional shear degradation of the generated flocs. Over the initial measurement time, this degradation would be most likely attributed to floc breakdown, while densification may also occur over longer timescales (Kyoda et al., 2019). To help understand these changes, additional measurements of average floc diameter and fractal dimension were taken for the flocculated suspensions over 300 s (data averaged in 30 s bins). Also, it is noted that whilst SLS has a natural bias to oversize particulates, the observed influence of shear on floc diameter is significant enough that the bias is likely negligible. Floc size distribution data were generated from the Mastersizer 2000E as Mie theory based SLS, using a 683 nm He-Ne laser via Eq. (12). For each experiment, the scattering intensity is a function of the magnitude of the scattering wave vector, Q , a reciprocal of the particle size,

where n is the refractive index, λ is the wavelength of the incident light in vacuo and θ is the scatter angle.

$$Q = \frac{4\pi n}{\lambda} \sin(\theta/2) \quad (12)$$

For determination of the fractal dimension, a particle that satisfies the Rayleigh-Gans-Debye criteria (Glover et al., 2000), the scattering intensity $I(Q)$ is given by Eq. (13):

$$I(Q) = kP(Q)S(Q) \quad (13)$$

where k is the scattering constant, $P(Q)$ is the single particle form factor and is related to the shape of the primary particle, and $S(Q)$ is the interparticle structure factor which describes the interference proposed by the primary particles within the aggregate. For a detailed analysis of light scattering theory within aggregates, see Sorensen (2001). Therefore, the fractal dimension of the flocs can be determined by plotting $\log I(Q)$ with respect to $\log Q$ (Sorensen, 2001) as per the following proportionality in Eq. (14) (Burns et al., 1997).

$$I(Q) \propto S(Q) \propto Q^{-d_f} \quad (14)$$

As noted, there was some potential for additional shear degradation (breakage and densification) of the generated flocs (Lu and Spielmant, 1985; Zhou and Franks, 2006). Therefore, an initial investigation of floc degradation rate was undertaken, observing average floc size and changes in fractal dimension within the Mastersizer dispersion cell over 9000 s to assess the impact of densification in the presence of shear. To reduce the effect of floc breakdown on skewing the d_{50} and d_{90} average floc sizes, one measurement was taken for multiple aliquots of the flocculated suspension, measuring the first recorded floc size after the induction period and averaged, rather than taking multiple measurements of the same sample which would progressively undergo shear, reducing floc size over the measurement period. Fractal data were obtained over a $\log(Q)$ range of $-1.84 \mu\text{m}^{-1}$ to $0.96 \mu\text{m}^{-1}$ corresponding to sizes of $69.2 \mu\text{m}$ to $0.11 \mu\text{m}$ respectively. The fractal dimension was determined by linear fitting optimised for the greatest coefficient of determination (R^2) to determine the boundaries of the linear region corresponding to D_f and D_p values, where the gradient is the fractal dimension. As fractal structures are assumed self-similar, this scaling approach from the average smallest repeating floc structure is assumed to be consistent across the floc population (Sorensen, 2001).

Visual microscopy was also utilised to confirm the size and morphology of aggregates produced from suspensions dosed with 20 ppm polymer concentration, using a Morphologi G3 (Malvern Panalytical Ltd.) automated single element microscope. Floc samples were prepared in the same manner as described above, whereupon samples were placed onto 4 microscope slides and analysed optically with 3 repeats. The number of flocs analysed ranged between 40,000 and 60,000 for each system to gain statistical significance. Data were analysed both in terms of circular equivalent diameters and aspect ratio.

The morphology of aggregate flocs was also confirmed using cryogenic scanning electron microscopy (Cryo-SEM). Again, samples were prepared in the same manner as described, before being sampled. Flocculated suspensions were then cryogenically frozen using liquid nitrogen, then sublimed for 10 min to remove the fro-

zen liquid and reveal the floc structures. The cryogenically frozen samples were then coated in iridium to reduce charging effects and analysed using an EVO MA15: variable pressure W SEM (Carl Zeiss AG).

It is finally noted that zeta potential measurement using electrophoresis were also attempted to understand the change in surface charge with polymer adsorption. However, the polymer flocculation led to sedimentation of flocs in the test cell resulting in poor correlation function fittings, and are therefore not reported. However, it was not deemed critical analysis for this current study, due to the focus on the overall influence of floc structures on sedimentation, rather than the specific surface chemistry changes from polymer-particle interactions.

3.4. Gravimetric sedimentation performance

Visual observation of suspension-supernatant boundary level change with time was used to measure the influence of polymer concentration on hindered settling rates. Again, 2.5 vol% $Mg(OH)_2$ suspensions were prepared in the agitated 1 l baffled reactor, as described in Section 3.2, with variable concentrations of the two polymers (5–20 ppm). Flocculated suspensions were then transferred to 1 l measuring cylinders of 61 mm diameter. The cylinders were inverted 5 times to evenly re-suspend flocs and the interfacial height was measured over time. The turbidity of the resultant supernatant was taken after 30 min of settling, at 5 cm below the air water interface, using a TN-100 turbidity meter (Eutech Instruments).

4. Results and discussion

4.1. Size and structure characterization of flocculated $Mg(OH)_2$

Fig. 1A(i) and A(ii) show the *in situ* floc growth kinetics of $Mg(OH)_2$, with addition of 5, 10 and 20 ppm 30% σ and 40% σ polymers respectively, where the converted FBRM volume based 50th percentile cumulative particle size (d_{50}) is presented over time. The data display several distinct flocculation events; being initial floc growth upon addition of polymer, a floc size maxima size at intermediate times, which then leads to a dominant floc breakage process under shear and dynamic floc growth-breakage equilibrium, as acknowledged by previous literature (Benn et al., 2018; Cobble Dick et al., 2014; Li et al., 2018; Raj et al., 2017, 2016; Vajihinejad and Soares, 2018). For both polymer suspensions, 1000 s was selected as the reactor residence time to be used for all further testing, being a time beyond the floc maxima, where the aggregate d_{50} were relatively stable. While such periods of shear are greater than would normally be employed in water treatment operations, for example, the 1000 s time period is also consistent with expected operational regimes in nuclear waste treatment (Grant et al., 2016). It is evident therefore that some significant shear degradation of the polymer flocs occurs with these conditions, though it is also clear that the 20 ppm polymer systems led to significantly larger aggregates than for lower concentrations, which is generally consistent with previous literature on similar polymers (Benn et al., 2018; Franks et al., 2005; Heath et al., 2006; Hunter et al., 2020; Nasser and James, 2006). Fig. 1B shows the cumulative frequency distribution of the floc population at 1000 s, for suspensions without polymer and with 20 ppm of 30% σ and 40% σ polymer. Both flocculated suspension distributions are similar, although sizes are slightly larger overall for the 30% σ system.

Fig. 2A presents the SLS PSD of the suspensions with no polymer, as well as addition of 30% σ and 40% σ polymers at 20 ppm. Consistent with the FBRM data, both flocculated suspensions have

similar size distributions, although again, the 30% σ system is larger. Fig. 2B shows SLS data displaying the log of the wave vector against the log of scattering intensity. The diameters of the minimum repeating floc diameter and corresponding primary particles within the structure, were determined using the procedure outlined by Sorenson (2001). D_f and D_p are represented by the upper and lower limits of the linear regime in Fig. 2B, determined by linear fitting optimised for the greatest coefficient of determination (R^2). As shown in Table 2, D_f and D_p were determined to be 6.74 μm and 0.28 μm respectively for the 30% σ 20 ppm system and 8.01 μm and 0.34 μm respectively for the 40% σ 20 ppm system. Using the linear regime of Fig. 2B and the proportionalities highlighted in Eq. (14), the fractal dimensions of the 30% σ and 40% σ systems were determined from the gradient of the linear fitting to be 2.07 and 2.09 respectively. Using Eq. (2), the structure prefactor was then determined to be ~ 0.65 (to 2 sig. figs.) for both systems, and the number of primary particles in a floc calculated using Eq. (1) to be 467 and 487 for the 30% σ and 40% σ systems respectively. Finally using Eqs. (3) and (4), the densities of the flocs were determined to be $\sim 1045 \text{ kg m}^{-3}$ and $\sim 1049 \text{ kg m}^{-3}$ for the 30% σ and 40% σ systems, thus highlighting a very open structure (given the particle phase density is 2340 kg m^{-3}). Such values are again consistent with similar flocculated dispersions previously investigated (Benn et al., 2018; Franks et al., 2005; Glover et al., 2000; Heath et al., 2006; Nasser and James, 2006) and are indicative of a highly fractal structure in both cases.

It should be noted that when SLS is used to identify fractal structure, it only identifies the fractal structure of the smallest repeating flocs in the system, where the fractal dimension is then assumed to be the same throughout the entire floc population, regardless of floc size (Sorensen, 2001). Previous work has investigated the application of multifractal floc analysis of lime softening floc formation (Vahedi and Gorczyca, 2014), although whilst the methodology allows for greater insight into the nuances of floc formation and how fractal dimension varies with floc size, the techniques are still very computationally intensive. Additionally, it is highlighted by the authors that more research is required to investigate how to best utilise the information obtained from the multifractal spectra, to incorporate the variable floc density and nonhomogeneous mass distribution of flocs into the floc settling models (Vahedi and Gorczyca, 2014).

Fig. 2C(i) shows the kinetic changes to the 50th percentile floc diameter and Fig. 2C(ii) the simultaneous densification indicated by the increasing fractal dimension over time for the same flocs. While some reduction is evident, further changes over longer times were considered relatively small, with the d_{50} for both flocculated systems reducing only on the order of 5% (with a corresponding increase in fractal dimension, indicating minor densification). However, it is noted that measurements were averaged over 30 s periods, after a certain induction time (typically > 1 min) from when the suspension was added in order to give the appropriate obscuration, which indicated the concentration of flocs was within the operating envelope of the Mastersizer. Thus, there was some potential for aggregate breakdown to occur before the initial measurement could be taken (within 30–60 s of adding flocculated samples to the Mastersizer cell). There are also some very minor discrepancies between the fractal dimension computed from the slope of Fig. 2B, and the fractal dimension reported in Fig. 2C(ii), which may be due to slight differences in sampling preparation. For Fig. 2B, sub-samples were taken from the settling cylinders after inversion (prior to settling analysis) while samples were taken directly from the flocculation reactor for the kinetics study (Fig. 2C). Thus, there may have been some variance in shear experienced by the samples, although the same trends regarding how polymer charge density affects floc structure are observed. It is also noted again that only

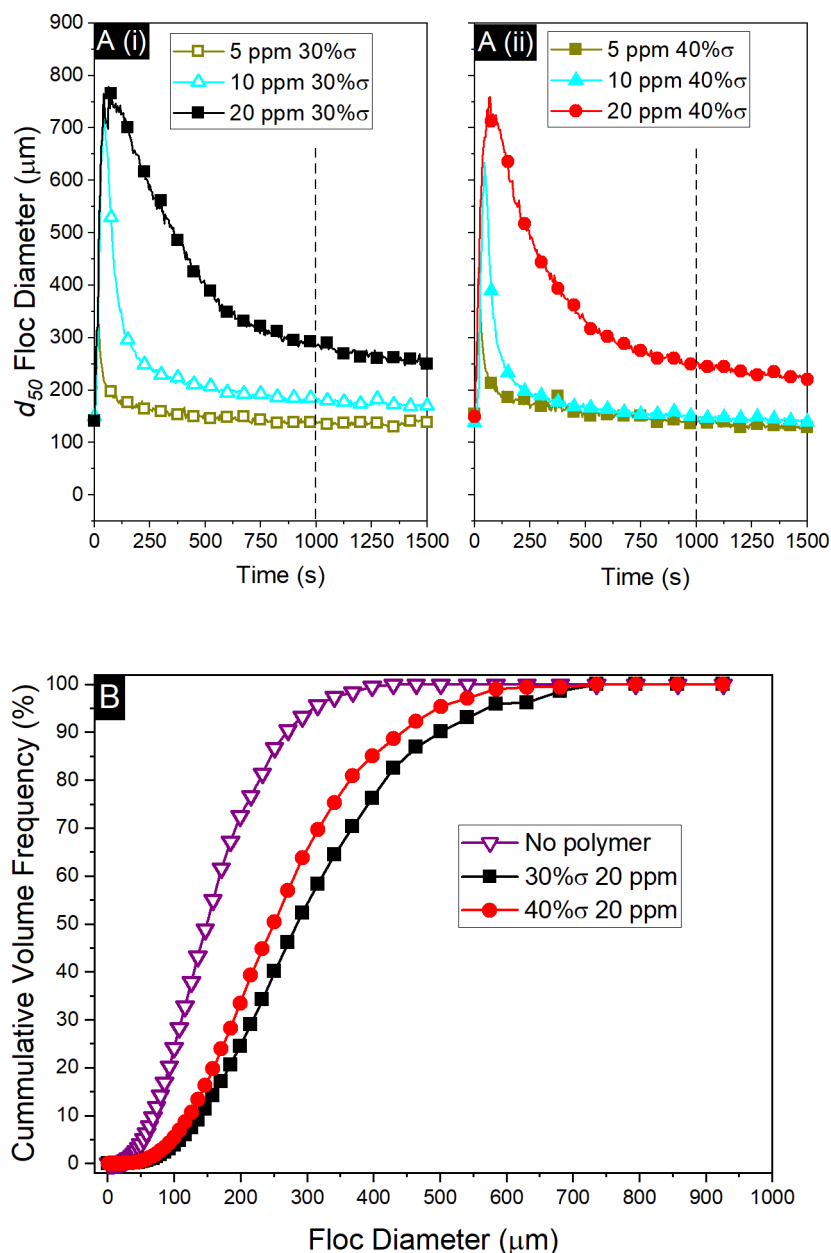


Fig. 1. A (i) & A (ii) Median volume weighted particle size (d_{50}) over time, measured with a focused beam reflectance meter (FBRM), for 2.5 vol.% $\text{Mg}(\text{OH})_2$ suspensions agitated at 300 rpm, flocculated with 30% σ and 40% σ anionic polymers respectively, dosed at 5, 10 and 20 ppm. Dashed vertical lines at 1000 s indicate mixing time used for equilibrium studies. B) Cumulative volume distribution of floc sizes for the same systems dosed at 20 ppm, measured by FBRM after 1000 s.

the initial 10 s average was used for fractal measurements in Fig. 2B (representing the ‘zero’ timepoint in Fig. 2C).

Fig. 3 presents quantified microscopy data (while Fig. 4 shows an example micrograph for 30% σ flocs) with 3A giving the aspect ratio distributions of the 30% σ and 40% σ polymer suspensions, demonstrating almost identical median aggregate aspect ratios of ~ 0.70 and ~ 0.69 respectively. Similar 2D morphologies have been previously reported (Chakrabarty et al., 2011) and are indicative of their fractal shape factors, given that for lower fractal dimensions, flocs assume a less symmetrical shape with elongation along a single plane (termed drag induced prolated flocs) (Chakrabarty et al., 2011). It is noted though, that their 2D shape factors will not necessarily be indicative of their 3D aspect ratios, due to flattening that can occur during drying on the microscopy slides.

The deviation from sphericity raises the question as to whether the aspect ratios influence shape effects (especially on fluid drag)

(see also Paul et al. (2017) and Winterwerp (1998)), and in turn compromise the validity of the proposed FMRZ model. If so, a shape factor variable may have to be introduced in predictive sedimentation equations (e.g., Eq. (10)), such as the coefficient used by Winterwerp (1998). For dilute sedimentation, a number of correlations exist to modify the drag coefficient for non-spherical particles (e.g. as used by Benn et al. (2018)), but for hindered settling additional drag manifests as differences in the Richardson-Zaki exponent, n (typically assumed as 4.65). For example, exponents >10 have been reported for high aspect ratio colloidal particles (Paul et al., 2017), due in part to achieving stable orientation with the flocs longest axis normal to the settling direction rather than parallel thus increasing fluid drag. However, for most systems of irregular particles with relatively low aspect ratio, exponent values of 5–6 are more common (Tomkins et al., 2005). Given that the measured values of circularity in the flocs (of ~ 0.7) do not suggest

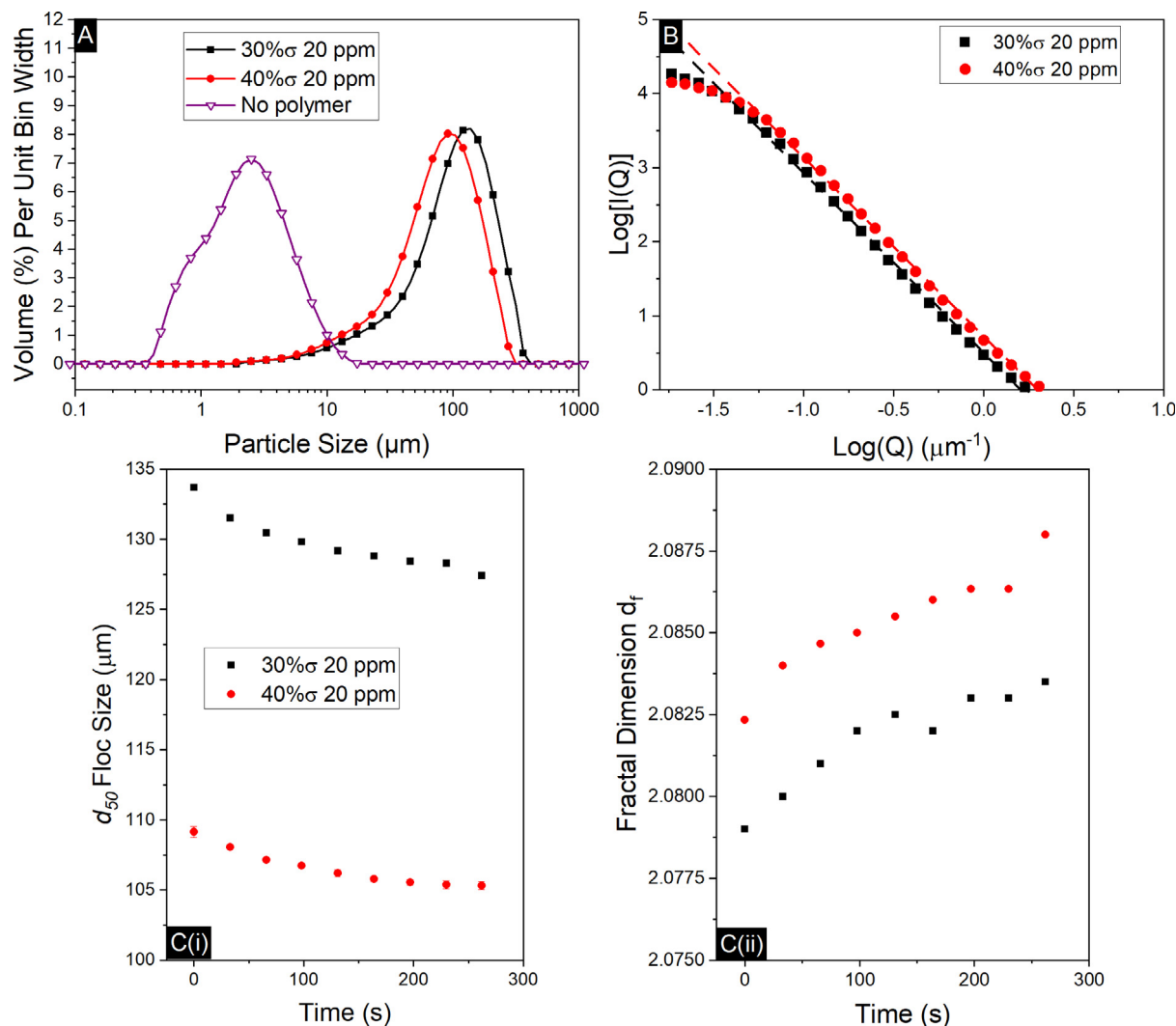


Fig. 2. (A) Static light scattering (SLS) particle size distributions of 2.5 vol.% Mg(OH)₂ suspensions with addition of 20 ppm 30%σ and 40%σ polymers, compared to sonicated Mg(OH)₂ with no polymer. Represented are continuous distributions for measurement bin sizes $\pm 6.25\%$ of the floating particle means. (B) SLS fractal dimension analysis of 2.5 vol.% Mg(OH)₂ suspensions with 30%σ and 40%σ polymer. (C) Kinetics of floc shear from shear degradation, showing (i) change in median diameter d_{50} with time and (ii) densification of Mg(OH)₂ with 20 ppm 30%σ and 40%σ polymers. All samples prepared in a reactor vessel at 300 rpm for 1000 s, then subsampled into the Malvern Mastersizer 2000E dispersion cell at 900 rpm.

Table 2

Calculated floc structural properties established from the minimum floc diameter (D_f) and the corresponding primary particle diameter (D_p) obtained from SLS (Fig. 2B). D_f and D_p were found by extracting the wave scatter vector (Q) reciprocals from the upper and lower limits of the linear regime (determined by linear fit) of $\log(IQ)$ vs. $\log(Q)$, where the fractal dimension (d_f) is the gradient of the linear trendline, indicated in Eq. (14). The structure prefactors (ψ) were calculated using Eq. (2), number of primary particles (N) in a floc were calculated using Eq. (1) and the volume fraction of particles in a floc (Φ_s) and floc densities (ρ_f) were calculated using Eqs. (3) and (4).

Properties determined from SLS data in Fig. 2B	30%σ 20 ppm	40%σ 20 ppm
Diameter of primary particle [D_p] (μm)	0.28	0.34
Diameter of minimum repeating flocs [D_f] (μm)	6.74	8.01
Floc fractal dimension [d_f]	2.07	2.09
Floc structure prefactor [ψ]	0.65	0.65
Number of particles in a floc [N]	469	487
Volume fraction of the particles in a floc [Φ_s]	0.034	0.037
Floc density [ρ_f] (kg m ⁻³)	1045	1049

highly asymmetrical form factors, it is likely therefore that any enhancement to the hindered settling exponent value would be relatively minor. In fact, Johnson et al. (2016) investigated the effect of altering the exponent value on predictions of coagulated

magnesium hydroxide aggregate sizes from settling data, where it was shown to be a mathematically weak dependency (with predicted sizes changing by < 9% as n was increased from 4.65 to 6). Further, it is important to emphasise the differences between discrete particles of a given shape and the greater volume occupation of fractal aggregates observed in zonal settling, which increases floc-floc perimeter interaction, thus enhancing drag to a significantly greater extent than particle shape factors (Paul et al., 2017).

Fig. 3B shows the cumulative frequency distribution of circular equivalent diameters from microscopy, while Table 3 gives the d_{50} and d_{90} values obtained from FBRM, SLS and optical microscopy methods. Table 3 also shows the calculated number of particles in the flocs measured by the aforementioned techniques based on the self-similar properties of the fractal flocs (Bushell et al., 2002). The solid particle volume fraction of the minimum repeating flocs (Φ_s) calculated using SLS data from Fig. 2B (~3.4 vol% and ~3.7 vol% for the 30%σ and 40%σ 20 ppm systems respectively) was used to calculate the number of particles from the measured polydisperse floc diameters by scaling up the number of particles in a minimum repeating floc in Table 2 using Eq. (15). Where \bar{N}_f is the number of particles in a measured polydisperse

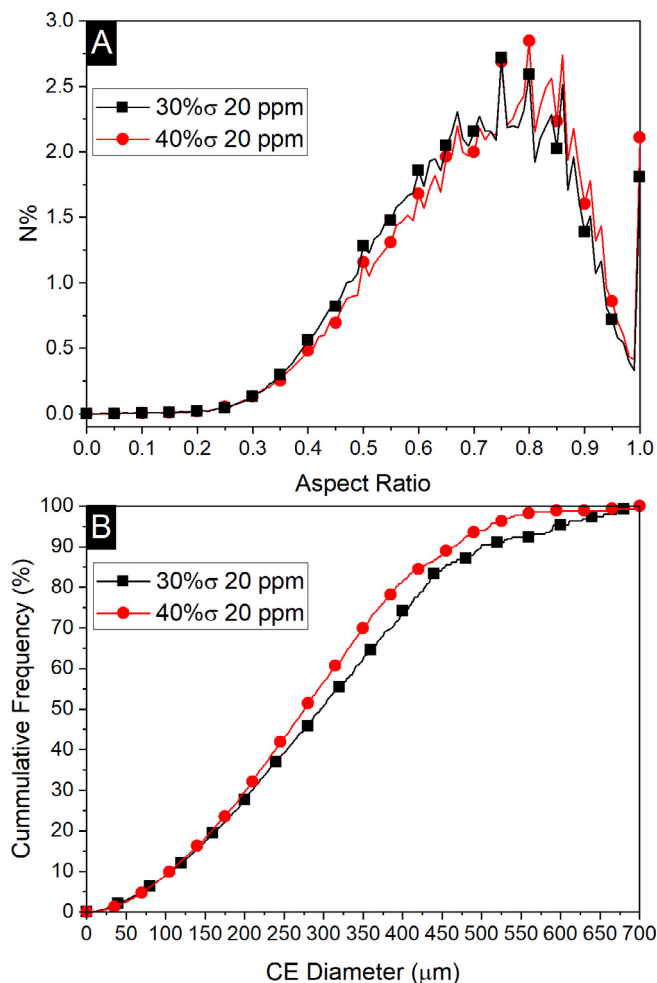


Fig. 3. (A) Aspect ratio distribution and (B) cumulative frequency distribution, for optical image analysis of 2.5 vol.% Mg(OH)₂ suspensions agitated for 1000 s at 300 rpm with 30%σ and 40%σ polymers dosed at 20 ppm.

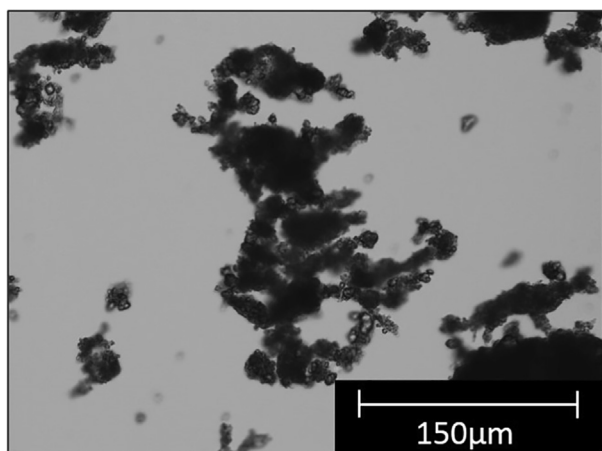


Fig. 4. Example optical microscope image of Mg(OH)₂ suspensions mixed with 20 ppm 30%σ polymer.

floc and \bar{V}_f is the spherical equivalent volume of measured polydisperse floc diameters (\bar{D}_f).

$$\bar{N}_f = (\bar{V}_f / V_p) \Phi_s \quad (15)$$

Table 3

Comparison of the 50th (d_{50}) and 90th (d_{90}) percentile equivalent polydisperse floc diameters, \bar{D}_f , using focused beam reflectance measurement (FBRM), static light scattering (SLS) and optical microscopy (Opt) techniques, for 30%σ and 40%σ polymer- Mg(OH)₂ systems at 2.5 vol.% dosed at 20 ppm polymer concentration. The calculated number of particles in the measured polydisperse flocs, \bar{N}_f , is also listed and calculated using Eq. (15). These data are complemented with aspect ratios obtained via optical microscopy.

Measurement	30%σ 20 ppm		40%σ 20 ppm	
	\bar{D}_f (μm)	\bar{N}_f (10 ⁷)	\bar{D}_f (μm)	\bar{N}_f (10 ⁷)
d_{50} (FBRM)	285	~3.6	245	~1.4
d_{90} (FBRM)	501	~19	437	~7.9
d_{50} (SLS)	134	~0.4	110	~0.1
d_{90} (SLS)	258	~2.6	214	~0.9
d_{50} (Opt)	295	~3.9	275	~2
d_{90} (Opt)	508	~20	463	~9.4
Aspect ratio (Opt)	0.7		0.69	

The calculated polydisperse floc particle numbers (\bar{N}_f) in Table 3 aid comparisons between the 30%σ and 40%σ 20 ppm systems, with regards to floc size and solid particle components. For a given size, an increase in particle number will increase the density of the floc, although as settling rate is a function of the square of floc size, increases in size will influence the measured rate to a greater degree. Importantly also, it is emphasised that a less dense floc with lower particle number (for a given size) infers a greater effective volume fraction of the flocs (see Eq. (15)) which itself will enhance hindered drag, potentially reducing settling rates. The microscopy data are consistent with FBRM and SLS measurements discussed, indicating that the lower charge density 30%σ polymer suspensions produced consistently larger flocs (and larger particle numbers) than the 40%σ polymer. Importantly also, whilst the differences in values of d_{50} are relatively small, there is a greater variation for the d_{90} floc diameter averages. This deviation between distribution values aligns with the research conducted by Nasser and James (2006), Zhou and Franks (2006) and Franks et al. (2005), who found that lower charge density polymers produce larger, less dense flocs, although differences in size and fractal dimension values are normally more pronounced in previous literature (Glover et al., 2000; Zhou and Franks, 2006). Generally, it has been shown that lower charge density polymers may conform on particle surfaces at a slower rate (Franks et al., 2005; Nasser and James, 2006; Zhou and Franks, 2006), producing larger flocs from the lower electrostatic driving force between the polymer functional groups and the particle charged surface. However, it appears in the current case, that the relatively small difference in polymer charge density results in relatively small overall differences in floc sizes, although, given the greater increase in d_{90} values for the 30%σ polymer systems, such differences may be great enough to produce variations in sedimentation behaviour.

In terms of instrumental variation, data in Table 3 show that SLS analysis measured considerably smaller d_{50} and d_{90} values for both systems, while values from FBRM and optical microscopy were similar. The differences in size for the SLS data are likely due to the shear occurring in the measurement cell, which demonstrate partial floc size degradation with time during agitation. As described, to prevent particle deposition and bubble formation, the SLS dispersion unit circulation rate was required to be a minimum of 900 rpm, which increases the shear from the baffled reactor system that the flocs were prepared in (300 rpm). While this enhanced shear did not appear to lead to pronounced size reduction over long time periods (as discussed in relation to Fig. 2C(i)) it is important to note, as detailed, that each measurement represents 10 s averages and does not include the induction time

required to produce acceptable obscuration in the cell. Hence, it is likely that the majority of the shear breakdown of the flocs occurred very rapidly, within the initial measurement time window.

The consistency between FBRM and optical microscopy data gives confidence that measured polydisperse floc sizes closely represent the actual aggregate distributions within the suspensions, and additionally highlights the stability of flocs to sampling. The close correlation is particularly important, given the limitations of each individual technique. For the optical system, flocs are laid out on one plane which may affect their orientation and thus maximum diameter, while subjecting them to capillary forces on the microscope slide. Alternatively, it is emphasised again that the FBRM actually measures particle chord lengths, rather than true diameters. Thus, results suggest the translation employed to convert sizes to volume averaged diameters is a very close fit to the data (Kyoda et al., 2019).

Optical microscopy images of the 30% σ polymer-Mg(OH)₂ floc dosed at 20 ppm, enable the fractal structure of the flocs to be inferred, and demonstrate the deviation from circularity, as quantified in Fig. 3A. Furthermore, closer observation indicates the presence of individual detached primary particles that can be seen around the flocs. Whilst particle detachment is likely in the transfer to microscope slides, if they occur within the suspension they may potentially generate increased turbidity if small enough to separate from the bulk suspension, as suggested by Johnson et al. (2016) in previous work on the sedimentation of Mg(OH)₂. Cryogenic scanning electron micrographs of a 40% σ polymer-Mg(OH)₂ floc (Fig. 5), highlight more detailed structures than the optical microscopy. The primary particles in the floc structures can be seen to be submicron platelets, as indicated by SEM imaging of the raw Mg(OH)₂ in Fig. S1. These structures resemble computational simulation designs of flocs of similar fractal dimensions (≈ 2.09) (Glover et al., 2000) in reaction limited cluster-cluster aggregation mechanisms of flocculation (de Martín et al., 2014; Xiao et al., 2013). In this process, large clusters of aggregated particles interact to form an even larger network floc, as opposed to particle by particle addition of the diffusion limited cluster-cluster aggregation mechanism (Jungblut et al., 2019). Given that Fig. 3A demonstrates similar aspect ratio and fractal dimension for both the 30% σ and 40% σ systems that also agree with aspect ratios found by Xiao et al. (2013) in computer simulated designs, it is likely that the reaction limited cluster-cluster aggregation mechanism is dominant in both 30% σ and 40% σ systems.

The significant porosity observed in Figs. 4 and 5, suggest that liquid permeability within the floc structures may be large enough to encompass smaller primary particle phases and axiomatically allow fluid flow through these micro channels in a similar manner to previous reports (Johnson et al., 2016; Xiao et al., 2013). Moreover, polymer chains linking the primary particles are present in the Cryo-SEM images, consistent with work completed by Sharma et al. (2017). Capturing images of cryogenically frozen polymer chains is generally very difficult, because of the sensitivity of the organic materials to electron bombardment (Sharma et al., 2017). Even at low voltages, this damage can be extensive. The chains found in the images are sparse on the particle surface and represent 'surviving' polymer chains that are much thicker than expected for single polymer segments. Sharma et al. (2017) have hypothesised that the variation in polymer chain dimension could be due to the stacking of fine polymer chains, giving rise to thicker structures, or due to the presence of poorly dissolved polymer, where the loss in water due to cryogenic freezing and sublimation leads to collapse and aggregation of the polymer network.

4.2. Measurement and prediction of floc sedimentation rates

Fig. 6A(i) and A(ii) present the change in the zonal interface height (mud-line) with time, for varying concentrations of both 30% σ and 40% σ polymers respectively, while Fig. 6B shows the average linear settling rate against varying polymer concentration for both systems. These data are also complemented with supernatant turbidity values after 30 min of sedimentation taken from 5 cm below the air-water interface (Fig. S5 within the ESM) where it was found that the 30% σ system reduced supernatant turbidity to a greater extent than the 40% σ system, although both produced very low turbidity values inferring efficient separation. As expected, the increase in polymer concentration resulted in a greater settling rate for both 30% σ and 40% σ polymers. This result also correlated to changes in aggregate size from FBRM (Fig. 1A) where the increase was most pronounced for the 30% σ system at 20 ppm concentration.

The validity of the FMRZ model (Eq. (10)) was demonstrated by comparing experimentally determined settling rates for the 20 ppm dosed 30% σ and 40% σ systems (Fig. 7A), to those predicted using measured d_{50} and d_{90} sizes from FBRM, SLS and optical microscopy, with fractal dimensions estimated from SLS data in Fig. 2B. The zonal settling rate predictions determined by the FMRZ model are also shown for comparison in ESM Figs. S6A and S6B, for

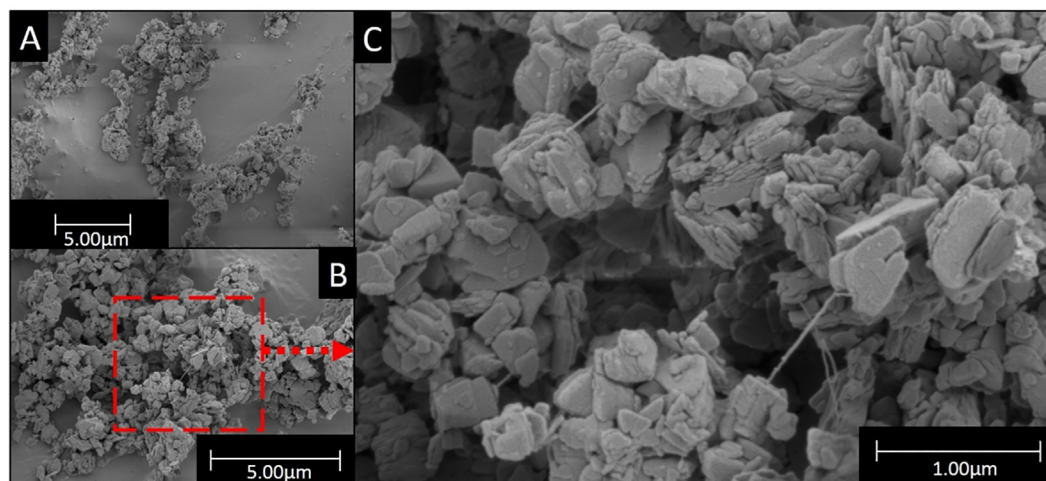


Fig. 5. Cryo-SEM images of 2.5 vol.% Mg(OH)₂ suspensions mixed with 20 ppm 40% σ polymer. (A) 19982x magnification, (B) 35000x magnification and (C) 99959x magnification.

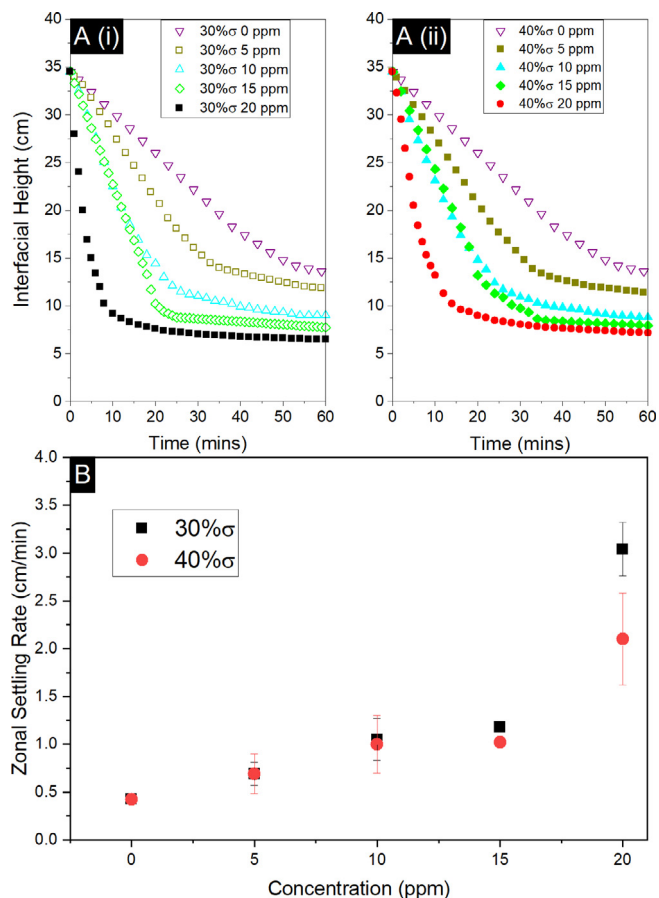


Fig. 6. (A) Interface height versus time for flocculated 2.5 vol.% Mg(OH)₂ with varying concentrations of (i) 30%σ and (ii) 40%σ polymer, prepared in a reactor agitated at 300 rpm for 1000 s. (B) Linear zonal settling rate versus polymer concentrations for the same systems.

the 30%σ and 40%σ 20 ppm system respectively. The same comparisons for a 10 ppm dose of both polymers are also given in the ESM, Fig. S7 (without the addition of optical microscopy measurements). Interestingly, the measured d_{50} values underpredicted the actual settling rates considerably in each case, where additionally, calculations based from SLS size data were poor, due to the assumed aggregate breakup. Settling rate predictions from FBRM and optical microscopy were much closer to experimental values when using the 90th percentile (d_{90}) values, especially for the 30%σ system. The same trends are evident for the 10 ppm data (Fig. S7) although, in general, the settling rate predictions are lower than the measured values (perhaps due to lower size measurement resolution, from the smaller particle sizes present). It is also noted that as the settling rate scales to the diameter squared, small deviations in size measurements will lead to large apparent errors in estimated settling rates. With both 10 and 20 ppm systems, critically, results suggest that the population of flocs that occupy only the top 10% of the total systems by size dominate the settling mechanics. A likely explanation for this behaviour is the ‘netting’ effect observed in sweeping flocculation (Ghernaout and Ghernaout, 2012; Jarvis et al., 2006; Shi et al., 2007). As larger, faster setting flocs sediment in the vertical plane, they may encompass slower settling, smaller flocs in their microstructure (possible given the size of such voids observed in microscopy data in Figs. 4 and 5) leading to densification and integration of the agglomerates (Johnson et al., 2016).

Previous studies that also found larger (d_{90}) sized flocs had a greater effect on sedimentation performance (Heath et al., 2006;

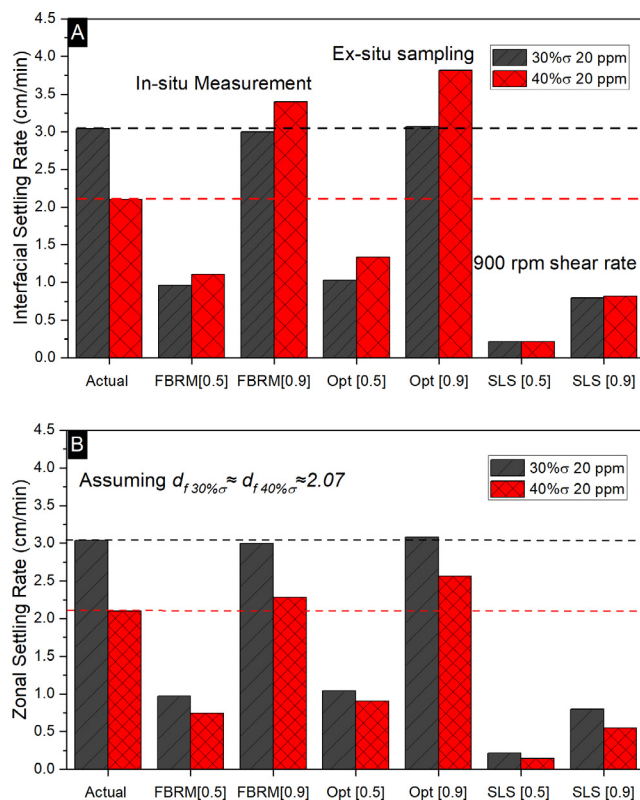


Fig. 7. (A) Comparison of measured (actual) zonal settling rates (dashed lines) for flocculated 2.5 vol.% Mg(OH)₂ suspensions mixed with 20 ppm 30%σ ($d_f = 2.07$) and 40%σ ($d_f = 2.09$) polymer, to those predicted by the fractal modified Richardson-Zaki equation (Eq. (10)). Comparisons using median [0.5] and 90th percentile [0.9] sizes measured by *in situ* focused beam reflectance meter (FBRM), *ex situ* optical microscopy (Opt) and *ex situ* static light scattering (SLS) that incorporated a 900 rpm agitated feed-cell. (B) Comparison of measured and predicted data as (A), assuming identical fractal properties for both flocculated polymer systems ($d_f = 2.07$).

Nasser and James, 2006), have examined a number of other mechanisms that may explain the observed behaviour, in addition to ‘netting’ interactions. What may also be important in high solid fraction systems, is the increased porosity of fractal aggregates, which may allow for microflow channels to relieve hydrodynamic stress across the projected surface of the floc, by producing a vector for fluid to flow through the fractal structure (Xiao et al., 2013). Such effects would be greater in larger flocs (and so more important for the d_{90} versus d_{50} sizes) as fractal floc densities may reduce with size, due to potential variability of fractal dimension with floc diameter. Any such variation would not be captured by SLS measurements, which assume self-repeating fractal structures (Glover et al., 2000; Sorensen, 2001; Vahedi and Gorczyca, 2014; Vahedi and Gorczyca, 2012; Vahedi and Gorczyca, 2011). Computational investigations by Xiao et al. (2013) into aggregates displaying a fractal dimension of 2.13, demonstrated such high levels of intra-aggregate permeability that the internal flow through the microstructure increased the settling rate of the bulk suspended solids significantly when compared to non-permeable controls. Further, studies by Johnson et al. (2016) on naturally coagulated Mg(OH)₂ also found evidence for the influence of fluid flow through rather than around settling aggregates. They observed that there was a sudden reduction in the hindered settling exponent at intermediate particle concentrations (indicative of reduced drag) which was hypothesized to occur when inter-aggregate spacing approached that of intra-aggregate spacing, due to the low density of particles within an aggregate. In such

cases, the assumption by Heath et al. (2006) that the magnitude of hindrance due to aggregate shape effects is negligible when compared to that of average hindered settling interactions due to the floc volume, is likely valid.

Further in Table 3, the calculated number of particles within the measured floc diameters is also recorded. Comparing the floc diameters and particle numbers for the d_{90} optical microscopy data, while the 30% σ system is $\sim 10\%$ larger by diameter than the 40% σ system, it contains more than twice the number of primary particles. Therefore, it would be expected that the larger, more particle loaded 30% σ flocs would sediment at a faster rate, due primarily to its increased floc density, as experimentally measured. However, in terms of the model prediction, this is not the case (as shown in Fig. 7A) where the predicted sedimentation rate for the 40% σ is actually greater. This disparity suggests that the hindering functionality of the FMRZ model (described by the fractal dimensionless permeability number, f_s^*) is particularly sensitive to small changes in fractal dimension, due to the significant weight that the FMRZ model in Eqn.10 places on fractal dimension values. While measured values for the 40% σ systems are slightly larger, differences between the flocs are minor (with $d_f = 2.09$ for 40% σ and 2.07 for 30% σ systems) and likely within experimental error. However, these differences correlate to relatively large differences in both predicted sedimentation rates and the calculated number of particles within a floc.

Thus, to test the influence of the fractal dimension, settling rate predictions were re-calculated, assuming both floc systems had a fractal dimension of 2.07, as per the 30% σ systems (given predictions were closer in this case). From this FMRZ modelling (Fig. 7B) it is evident that the 40% σ system predictions are now below that of the 30% σ system and align much closer to the experimental rates (at least for those estimated on the d_{90} sizes). In terms of floc particle numbers, assuming the fractal dimension is lower than measured, and using the fractal dimension 2.07 in lieu of 2.09 (assuming a fixed D_f/D_p ratio) results in a decrease to the number of particles in a minimum repeating floc. Indeed, the resultant polydisperse floc number for the 40% σ system is reduced from $\sim 9.4 \times 10^7$ to $\sim 8.8 \times 10^7$ (a 6% reduction), which in turn translates to a $\sim 33\%$ reduction in zonal settling rate. This result highlights that the actual fractal dimensions of the two flocculated systems are remarkably similar, but also, that model predictions are extremely sensitive to fractal dimension values. Therefore, it is important that fractal dimensions can be estimated accurately and use of a low-shear dispersion cell would be recommended for future work.

To further understand the influence of FMRZ model parameters on output predictions, a multivariate analysis of the FMRZ model was conducted, as shown in Fig. 8. Fig. 8A demonstrates how both changes in floc diameter and fractal dimension affect the predicted zonal settling rates, where measured SLS and Opt d_{50} and d_{90} data (for both 30% σ and 40% σ systems) have been added onto the FMRZ surface plot for comparison. Fig. 8B presents the variation of polydisperse floc particle number with fractal dimension, for arbitrary floc diameters of 100, 500 and 900 μm , selected to cover the experimental range. The limits of the fractal analysis, in terms of Eq. (9), are that the effective floc volume fraction, ϕ_f , must also be less than 1. Therefore, the fractal dimension limit for Eq. (9) to be valid, was determined by fitting of the calculated change in effective volume fraction for different fractal dimension values (see ESM Fig. S8). Here, $\phi_p = 0.025$ and D_f and D_p are fixed for their respective charge density polymer systems shown in Table 2, and was found to be $1.84 \leq d_f$.

It is evident from Fig. 8A (as also highlighted in Fig. 7B) that even small increases in fractal dimension result in considerable changes to settling velocity, and those effects are much more significant than changes to aggregate size (noting fractal dimension

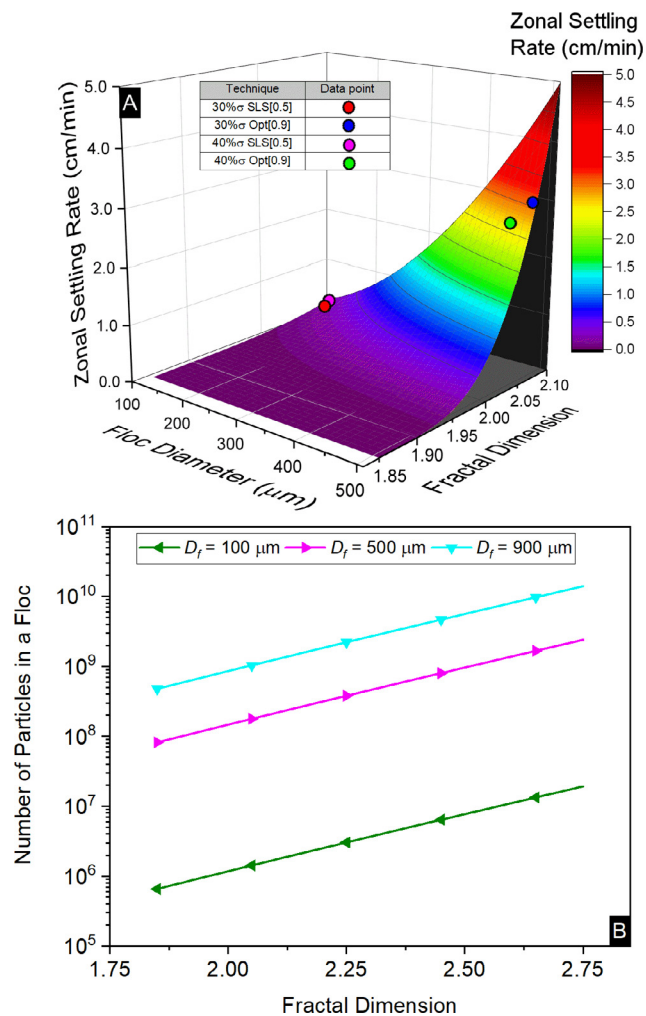


Fig. 8. (A) FMRZ model prediction of the zonal settling rate of 2.5 vol.% Mg(OH)₂ suspensions mixed with 20 ppm 30% σ polymer, for various input floc sizes, D_f , and fractal dimensions, d_f , based on the fractal modification of the Richardson-Zaki equation (Eq. (10)). Here, $\rho_p = 2340.6 \text{ kg m}^{-3}$, $\rho_w = 1000 \text{ kg m}^{-3}$, $g = 9.81 \text{ m s}^{-2}$, $\mu_w = 8.9 \times 10^{-4} \text{ kg m}^{-1} \text{ s}^{-1}$, $D_f = 6.74 \mu\text{m}$ and $D_p = 0.28 \mu\text{m}$. (B) The change in the floc particle number, N_f , as a function of floc diameter and fractal dimension for $D_f = 100, 500$ and $900 \mu\text{m}$, selected to cover the experimental range.

is only varied between 1.85 and 2.1, while floc sized is increased from 100 to 500 μm). The reason for this functional influence, is due to the non-linear effects on the effective volume fraction, ϕ_f , of the flocs. The isolated function representing the change in the dimensionless permeability number, f_s^* , with increasing fractal dimension, was found to be highly non-linear (see, ESM Fig. S9). Conversely, large changes in the fractal dimension (1.85–2.75) were less impactful on the particle number within flocs, than the changes to the overall floc sizes (see Fig. 8B) consistent with the order reported experimentally in Table 3. Only in the case where the fractal dimension, d_f , approaches 3 (resulting in the effective volume fraction, ϕ_f , approaching the initial particle volume fraction, ϕ_p) does the impact of the measured floc diameter, \bar{D}_f , and thus the Stokes function of the FMRZ model, become dominant in determining the settling rate of the suspension.

Furthermore, Table 4 displays analysis conducted to determine the corresponding predicted fractal dimension values for each of the measured floc diameters in Table 3 (using the FMRZ model) to produce the experimentally determined zonal settling rates in Fig. 6A and 6B. The inverse was also computed in Table 4 to give

Table 4

Interpolated fractal dimensions from the FMRZ model (Eq. (10)) for experimentally obtained floc diameters (in Table 3) to project the experimentally obtained zonal settling rates in Fig. 6A and B. Also given is the corresponding interpolated floc diameters required to project the experimental zonal settling rates, based on the experimentally obtained fractal dimension data (Fig. 2B).

Measurement	Corresponding modelled fractal dimension	
	30% σ 20 ppm	40% σ 20 ppm
d_{50} (FBRM)	2.15	2.14
d_{90} (FBRM)	2.07	2.07
d_{50} (SLS)	2.31	2.31
d_{90} (SLS)	2.17	2.17
d_{50} (Opt)	2.14	2.13
d_{90} (Opt)	2.07	2.06
Corresponding modelled floc diameter	505 μm	357 μm

floc size predictions for the measured fractal dimensions (in Fig. 2B). These data further highlight the non-linear influence of the fractal dimension, when considering the d_{50} (SLS) data measured in Table 3, which represents the furthest departed prediction from the experimentally measured zonal settling rates for both the 30% σ and 40% σ 20 ppm systems.

For the 30% σ system, the FMRZ modelled sedimentation rate based on the SLS experimentally obtained d_{50} floc diameters and fractal dimensions, is over 20 times lower than the experimentally observed zonal settling rate. When extracting the corresponding polydisperse floc diameter from the FMRZ model based on the experimentally obtained fractal dimension of 2.07 to predict the experimentally obtained zonal settling rate, the SLS d_{50} diameter in Table 3 is increased almost fivefold from 134 μm to 505 μm (shown in Table 4). However, when performing the inverse, where the corresponding fractal dimension is extracted from the measured d_{50} SLS floc diameter to predict the experimentally obtained zonal settling rate, only an increase of 2.07 to 2.31 (or $\sim 10\%$) was required to achieve the same zonal settling rate increase. In terms of changes to floc particle numbers between these two scenarios, increasing the particle size to the estimated 505 μm results in a particle number increase from 0.37×10^7 to 20×10^7 (calculated using Eq. (15)). Alternatively, altering the fractal dimension to 2.31 would produce floc particle numbers in the order of just 0.92×10^7 . The comparative increase in zonal settling rate when comparing the change in the number of particles in flocs as a function of floc size and fractal dimension independently (Fig. 8B) further demonstrates that the zonal settling rate is greatly dependent on the fractal modified dimensionless permeability number (f_s^*). Small increases in fractal dimension non-linearly increase the dimensionless permeability number (see ESM fig. S9) producing greater zonal settling rates than increasing floc size. Essentially, increases in permeability number is reflective of decreases to the effective volume fraction of the dispersion. A high permeability number indicates the flocs take up a small effective volume, significantly decreasing overall drag from hindered settling. This influence of fractal dimension is more influential mathematically on estimated settling rates than increased floc weight granted by greater particle loading or larger floc sizes. However, as previously discussed, the dominance of fractal dimension is not reflected in the experimental work in Fig. 6A and 6B or by previous literature, where it has been observed that floc size is usually dominant in sedimentation performance (Heath et al., 2006; Nasser and James, 2006).

For the FMRZ model, when $\phi_p \left(\frac{D_f}{D_p}\right)^{3-d_f} \ll 1$, f_s^* is close to unity, and \bar{D}_f has a greater influence on zonal settling rate. Conversely, when $f_s^* \ll 1$, $\phi_p \left(\frac{D_f}{D_p}\right)^{3-d_f}$ is close to unity, and the zonal settling rate

is much more sensitive to values of d_f . The FMRZ model indicates that the 30% σ and 40% σ systems have f_s^* values of 0.05 and 0.07 respectively, suggesting that they are in a strongly hindered settling regime and more sensitive to fractal dimension than floc size. Since this was not strictly observed experimentally (with measured sedimentation rate being most dependent on d_{90} sizes) it indicates that the hindering effects are reduced in comparison to model estimates. In particular, the FMRZ model does not take into account any specific factors, for example, the effects of floc microstructure and internal porosity, as previously discussed. Aggregate porosity may provide a means of intra-aggregate flow, thus increasing the effective permeability number, f_s^* , closer to unity, enhancing the relevance of \bar{D}_f on zonal settling rates. Particularly, as suggested by Johnson et al. (2016), whilst the external perimeters of the flocs may interact through increased inter-aggregate packing, microflow channels in the flocs may prevent increased drag and boundary layer separation providing a vector for dewatering processes to dominate. Further, internal floc permeability hindering relief effects may be captured by theoretical models on aggregate densification and their impact on thickener performance, as suggested by Usher et al. (2009), which has been applied to batch settling and thickening scenarios similar to this work (Grassia et al., 2014; van Deventer et al., 2011; Zhang et al., 2013). Nevertheless, given these limitations, the correlation between predicted and experimental settling rates demonstrated in Figs. 7B and 8A, highlights that the FMRZ model still provides a close first approximation to experimental aggregate sedimentation rates.

It is lastly evident that the volume translation of the *in situ* FBRM measurements provided a very close size estimate, indicating the potential to couple inline measurements with the FMRZ model predictions, for process optimization and control of industrial solid-liquid separators. While, currently, there are no standard *in situ* techniques to easily measure aggregate fractal dimensions, it may simply be sufficient in most circumstances to evaluate fractal dimension using FMRZ model predictions from batch sedimentation data (as completed in Table 4) providing robust estimates of floc structures for full scale operations. There may also be the potential to combine model predictions with other *in situ* techniques, such as acoustic backscatter systems, to gain both size and structure information, completely negating the need for sampling (Bux et al., 2019). The sensitivity analysis of the FMRZ model presented in Fig. 8, is also critical for accurate integration into CFD simulations of clarifiers and thickeners, where similar fractal models are often used to simplify solid-liquid separation physics. The influence of uncertainties with fractal dimension values has, in particular, been shown to impact the accuracy of CFD predictions in simulations of large-scale flocculated calcite separation (Hunter et al., 2020).

5. Conclusions

This study investigated the flocculation of magnesium hydroxide dispersions with 30% and 40% charge density polyacrylamide-poly(acrylic acid) flocculants and resultant sedimentation behaviour. Static light scattering (SLS), focused beam reflectance measurement (FBRM) and automated optical microscopy found relatively small differences in resultant floc density, shape and size (although, SLS underpredicted floc sizes in all cases). Additionally, the 30% charge systems were measured to be slightly larger under all techniques, potentially due to a lower electrostatic driving force between polymer functional groups and the particle surface, resulting in slower conformation kinetics. Cryogenic scanning electron microscopy was also used to investigate floc microstructure, displaying porosity at multiple length scales.

Measured sedimentation rates were compared to estimations from a fractal modified Richardson-Zaki settling model (FMRZ model), to assess the role of floc size dominance in hindered sedimentation. It was found that the 90th cumulative percentile (d_{90}) floc sizes predicted settling rates more accurately than the d_{50} sizes, which was assumed to be due to netting effects. A full sensitivity study of the FMRZ model was also performed, indicating the valid fractal dimension range, and most importantly, the relative influence of floc size and fractal dimension parameters (along with associated particle number density in each floc). The correlation of settling rate predictions to experimental values (when using the d_{90} floc size) highlighted the advantages of the FMRZ model as a relatively simple method to achieve close first approximations, even though shape and internal porosity effects are not included. Additionally, the close correlation of FBRM size data when converted to a volume-based distribution, indicated its suitability as an *in situ* sizing technique to couple with FMRZ model estimations, for online prediction in industrial clarifiers and thickeners. Nevertheless, due to heavier weighting on floc compactness rather than the comparative floc particle loading - settling rate predictions were found to be overly sensitive to fractal dimension values from multivariate analysis, and likely above the sensitivity of the actual measurements. This result draws attention to the need for improved *in situ* methods of fractal dimension characterisation.

CRedit authorship contribution statement

Alexander P.G. Lockwood: Investigation, Methodology, Data curation, Formal analysis, Writing - original draft. **Jeffrey Peakall:** Conceptualization, Methodology, Formal analysis, Supervision, Funding acquisition, Writing - review & editing. **Nicholas J. Warren:** Conceptualization, Methodology, Formal analysis, Supervision, Writing - review & editing. **Geoff Randall:** Conceptualization, Project administration, Funding acquisition, Writing - review & editing. **Martyn Barnes:** Conceptualization, Project administration, Data curation, Writing - review & editing. **David Harbottle:** Conceptualization, Methodology, Supervision, Writing - review & editing. **Timothy N. Hunter:** Conceptualization, Methodology, Investigation, Validation, Funding acquisition, Writing - review & editing.

Declaration of Competing Interest

The authors declare that they have no known competing financial interests or personal relationships that could have appeared to influence the work reported in this paper.

Acknowledgements

The authors would like to thank the Engineering and Physical Sciences Research Council (EPSRC) U.K. and Sellafield Ltd for funding this research through the Centre for Doctoral training in Next Generation Nuclear (NGN-CDT) [EP/L015390/1]. We would also like to thank Stuart Mickelthwaite and the Leeds Electron Microscopy and Spectroscopy (LEMAS) Centre for their assistance and guidance with the cryogenic scanning electron microscope experiments. Finally, the authors would like to thank the anonymous reviewers for their important comments and suggestions that helped improve the paper.

Notes

The article metadata is available from the University of Leeds Research Repository; <https://doi.org/10.5518/923>. Article meta-

data is available under a Creative Commons Attribution licence (CC-BY).

Appendix A. Supplementary material

Supplementary data to this article can be found online at <https://doi.org/10.1016/j.ces.2020.116274>.

References

- Adachi, Y., Tanaka, Y., 1997. Settling velocity of an aluminium-kaolinite floc. *Wat. Res.* 31, 449–454.
- Adelman, M.J., Hurst, M.W., Weber-Shirk, M.L., Cabrito, T.S., Somogyi, C., Lion, L.W., 2013. Floc roll-up and its implications for the spacing of inclined settling devices. *Environ. Eng. Sci.* 30, 302–310. <https://doi.org/10.1089/ees.2012.0295>.
- Barlow, S.T., Stennett, M.C., Hand, R.J., Morgan, S.P., Hyatt, N.C., 2016. Thermal Treatment of UK Magnox Sludge, in: 2nd Petrus-OPERA PhD and Early Stage Researcher Conference, 2016.
- Barrett, P., Glennon, B., 2002. Characterizing the metastable zone width and solubility curve using lasentec FBRM and PVM. *Chem. Eng. Res. Des.* 80, 799–805. <https://doi.org/10.1205/026387602320776876>.
- Benn, F.A., Fawell, P.D., Halewood, J., Austin, P.J., Costine, A.D., Jones, W.G., Francis, N.S., Druett, D.C., Lester, D., 2018. Sedimentation and consolidation of different density aggregates formed by polymer-bridging flocculation. *Chem. Eng. Sci.* 184, 111–125. <https://doi.org/10.1016/j.ces.2018.03.037>.
- Biggs, S., Nabi, R., Poole, C., Patel, A., 2007. The Influence of Zeta Potential and Yield Stress on the Filtration Characteristics of a Magnesium Hydroxide Simulant, in: 11th International Conference on Environmental Remediation and Radioactive Waste Management, Parts A and B. ASME, pp. 1133–1139. <https://doi.org/10.1115/ICEM2007-7071>.
- Brostow, W., Hagg Lobland, H.E., Pal, S., Singh, R.P., 2009. Polymeric flocculants for wastewater and industrial effluent treatment. *J. Mater. Educ.* 31, 157–166.
- Burns, J.L., Yan, Y.-D., Jameson, G.J., Biggs, S., 1997. A light scattering study of the fractal aggregation behavior of a model colloidal system. *Langmuir* 13, 6413–6420.
- Bushell, G.C., Yan, Y.D., Woodfield, D., Raper, J., Amal, R., 2002. On techniques for the measurement of the mass fractal dimension of aggregates. *Adv. Colloid Interface Sci.* 95, 1–50.
- Bux, J., Peakall, J., Rice, H.P., Manga, M.S., Biggs, S., Hunter, T.N., 2019. Measurement and density normalisation of acoustic attenuation and backscattering constants of arbitrary suspensions within the Rayleigh scattering regime. *Appl. Acoust.* 146, 9–22. <https://doi.org/10.1016/j.apacoust.2018.10.022>.
- Camenen, B., Pham Van Bang, D., 2011. Modelling the settling of suspended sediments for concentrations close to the gelling concentration. *Cont. Shelf Res.* 31, 106–111. <https://doi.org/10.1016/j.csr.2010.07.003>.
- Cao, F., Miao, M., Yan, P., 2018. Effects of reactivity of MgO expansive agent on its performance in cement-based materials and an improvement of the evaluating method of MEA reactivity. *Constr. Build. Mater.* 187, 257–266. <https://doi.org/10.1016/j.conbuildmat.2018.07.198>.
- Chakrabarty, R.K., Garro, M.A., Garro, B.A., Chancellor, S., Moosmüller, H., Herald, C. M., 2011. Simulation of aggregates with point-contacting monomers in the cluster-dilute regime. Part 2: Comparison of two- and three-dimensional structural properties as a function of fractal dimension. *Aerosol Sci. Technol.* 45, 903–908. <https://doi.org/10.1080/02786826.2011.568022>.
- Cobbleck, J., Nguyen, A., Latulippe, D.R., 2014. Demonstration of FBRM as process analytical technology tool for dewatering processes via CST correlation. *Water Res.* 58, 132–140. <https://doi.org/10.1016/j.watres.2014.03.068>.
- Costine, A., Cox, J., Travaglini, S., Lubanski, A., Fawell, P., Misslitz, H., 2018. Variations in the molecular weight response of anionic polyacrylamides under different flocculation conditions. *Chem. Eng. Sci.* 176, 127–138. <https://doi.org/10.1016/j.ces.2017.10.031>.
- de Martín, L., Fabre, A., Ruud van Ommen, J., 2014. The fractal scaling of fluidized nanoparticle agglomerates. *Chem. Eng. Sci.* 112, 79–86. <https://doi.org/10.1016/j.ces.2014.03.024>.
- Elliott, L.N., Bourne, R.A., Hassanpour, A., Edwards, J.L., Sutcliffe, S., Hunter, T.N., 2018. Salt enhanced solvent relaxation and particle surface area determination via rapid spin-lattice NMR. *Powder Technol.* 333, 458–467. <https://doi.org/10.1016/j.powtec.2018.04.050>.
- Font, R., Pérez, M., 2000. Hydrodynamic parameters from the Michaels and Bolger method. *Chem. Eng. J.* 80, 167–175.
- Franks, G.V., Yates, P.D., Lambert, N.W.A., Jameson, G.J., 2005. Aggregate size and density after shearing, implications for dewatering fine tailings with hydrocyclones. *Int. J. Miner. Process.* 77, 46–52. <https://doi.org/10.1016/j.minpro.2005.02.002>.
- Ghernaout, D., Ghernaout, B., 2012. Sweep flocculation as a second form of charge neutralisation—a review. *Desalin. Water Treat.* 44, 15–28. <https://doi.org/10.1080/19443994.2012.691699>.
- Glover, S.M., Yan, Y., Jameson, G.J., Biggs, S., 2000. Bridging flocculation studied by light scattering and settling. *Chem. Eng. J.* 80, 3–12. [https://doi.org/10.1016/S1383-5866\(00\)00071-X](https://doi.org/10.1016/S1383-5866(00)00071-X).
- Gmachowski, L., 1995. Mechanism of shear aggregation. *Water Res.* 29, 1815–1820.

- Grant, I., Weintrager, U., Richardson, I.E., Wilson, D., 2016. Sellafield FGMSF additional sludge retrievals a significant step in decommissioning part of the U. K.'s Nuclear Legacy -16180, in: Waste Management Symposium. Phoenix, Arizona, USA.
- Grassia, P., Zhang, Y., Martin, A.D., Usher, S.P., Scales, P.J., Crust, A.H., Spehar, R., 2014. Effects of aggregate densification upon thickening of Kynchian suspensions. *Chem. Eng. Sci.* 111, 56–72. <https://doi.org/10.1016/j.ces.2014.02.013>.
- Gregory, J., 2009. Monitoring particle aggregation processes. *Adv. Colloid Interface Sci.* 147, 109–123.
- Gregory, J., 1988. Polymer adsorption and flocculation in sheared suspensions. *Colloids Surf.* 31, 231–253.
- Guan, Lei, Yuan, Zhulin, Moghtaderi, Behdad, Peng, Zhengbiao, Evans, Geoffrey M., Gu, Conghui, Doroodchi, Elham, 2020. Prediction of terminal velocity of fractal aggregates with IBM-LBM method. *Powder Technology* 361, 1060–1069. <https://doi.org/10.1016/j.powtec.2019.10.089>. In press.
- Guérin, L., Frances, C., Liné, A., Coufort-Saujéaud, C., 2019. Fractal dimensions and morphological characteristics of aggregates formed in different physico-chemical and mechanical flocculation environments. *Colloids Surfaces A Physicochem. Eng. Asp.* 560, 213–222. <https://doi.org/10.1016/j.colsurfa.2018.10.017>.
- Hallam, K.R., Minshall, P.C., Heard, P.J., Flewitt, P.E.J., 2016. Corrosion of the alloys Magnox AL80, Magnox ZR55 and pure magnesium in air containing water vapour. *Corros. Sci.* 112, 347–363. <https://doi.org/10.1016/j.corsci.2016.07.033>.
- Heath, A.R., Bahri, P.A., Fawell, P.D., Farrow, J.B., 2006. Polymer flocculation of calcite: relating the aggregate size to the settling rate. *AIChE J.* 52, 1987–1994. <https://doi.org/10.1002/aic.10789>.
- Heath, P.G., Stewart, M.W.A., Moricca, S., Hyatt, N.C., 2018. Hot-isostatically pressed wasteforms for Magnox sludge immobilisation. *J. Nucl. Mater.* 499, 233–241. <https://doi.org/10.1016/j.jnucmat.2017.11.034>.
- Hogg, R., 2013. Bridging Flocculation by Polymers. *KONA Powder Part. J.* 30, 3–14.
- Hunter, T.N., Peakall, J., Egarr, D., Cowell, D.M.J., Freear, S., Tonge, A.S., Horton, L., Rice, H.P., Smith, I., Malone, K., Burt, D., Barnes, M., Randall, G., Biggs, S., Fairweather, M., 2020. Concentration profiling of a horizontal sedimentation tank utilising a bespoke acoustic backscatter array and CFD simulations. *Chem. Eng. Sci.* 218, <https://doi.org/10.1016/j.ces.2020.115560> 115560.
- Jackson, S.F., Monk, S.D., Riaz, Z., 2014. An investigation towards real time dose rate monitoring, and fuel rod detection in a First Generation Magnox Storage Pond (FGMSF). *Appl. Radiat. Isot.* 94, 254–259. <https://doi.org/10.1016/j.apradiso.2014.08.019>.
- Jarvis, P., Jefferson, B., Parsons, S.A., 2006. Floc structural characteristics using conventional coagulation for a high doc, low alkalinity surface water source. *Water Res.* 40, 2727–2737. <https://doi.org/10.1016/j.watres.2006.04.024>.
- Johnson, M., Peakall, J., Fairweather, M., Biggs, S., Harbottle, D., Hunter, T.N., 2016. Characterization of multiple hindered settling regimes in aggregated mineral suspensions. *I&EC Res.* 55, 9983–9993. <https://doi.org/10.1021/acs.iecr.6b02383>.
- Joseph-Soly, S., Saldanha, T., Nosrati, A., Skinner, W., Addai-Mensah, J., 2019. Improved dewatering of clay rich mineral dispersions using recyclable superabsorbent polymers. *Chem. Eng. Res. Des.* 142, 78–86. <https://doi.org/10.1016/j.cherd.2018.07.032>.
- Jungblut, S., Joswig, J.-O., Eychmüller, A., 2019. Diffusion- and reaction-limited cluster aggregation revisited. *Phys. Chem. Chem. Phys.* 21, 5723–5729. <https://doi.org/10.1039/C9CP00549H>.
- Khelifa, A., Hill, P.S., 2006. Models for effective density and settling velocity of flocs. *J. Hydraul. Res.* 44, 390–401.
- Kim, S., Palomino, A.M., 2009. Polyacrylamide-treated kaolin: a fabric study. *Appl. Clay Sci.* 45, 270–279. <https://doi.org/10.1016/j.clay.2009.06.009>.
- Kinoshita, T., Nakaishi, K., Kuroda, Y., 2017. Determination of kaolinite floc size and structure using interface settling velocity. *Appl. Clay Sci.* 148, 11–16. <https://doi.org/10.1016/j.clay.2017.07.024>.
- Krysiak-Baltyń, Konrad, Cavalida, Raul, Thwaites, Ben, Reeve, Petra J., Scales, Peter J., Van den Akker, Ben, Ong, Lydia, Martin, Gregory J.O., Stickland, Anthony D., Gras, Sally L., 2019. Comparison of physical characteristics and dewatering behaviour between granular and floccular sludges generated from the same seawage. *Journal of Water Process Engineering* 29, 100785. <https://doi.org/10.1016/j.jwpe.2019.100785>. In press.
- Kyoda, Y., Costine, A.D., Fawell, P.D., Bellwood, J., Das, G.K., 2019. Using focused beam reflectance measurement (FBRM) to monitor aggregate structures formed in flocculated clay suspensions. *Miner. Eng.* 138, 148–160. <https://doi.org/10.1016/j.mineng.2019.04.045>.
- Li, H., Liu, M., Liu, Q., 2018. The effect of non-polar oil on fine hematite flocculation and flotation using sodium oleate or hydroxamic acids as a collector. *Miner. Eng.* 119, 105–115. <https://doi.org/10.1016/j.mineng.2018.01.004>.
- Li, Mingzhong, Wilkinson, Derek, 2005. Determination of non-spherical particle size distribution from chord length measurements. Part 1: Theoretical analysis. *Chemical Engineering Science* 60 (12), 3251–3265. <https://doi.org/10.1016/j.ces.2005.01.008>. In press.
- Liao, J.Y.H., Selomulya, C., Bushell, G., Bickert, G., Amal, R., 2005. On Different approaches to estimate the mass fractal dimension of coal aggregates. *Part. Part. Syst. Charact.* 22, 299–309. <https://doi.org/10.1002/ppsc.200500978>.
- Lu, C.F., Spielmant, L.A., 1985. Kinetics of Floc breakage and aggregation in agitated liquid suspensions. *Colloid Interface Sci.* 103, 95–105.
- Maher, Z., Ivanov, P., O'Brien, L., Sims, H., Taylor, R.J., Heath, S.L., Livens, F.R., Goddard, D., Kellet, S., Rand, P., Bryan, N.D., 2016. Americium and plutonium association with magnesium hydroxide colloids in alkaline nuclear industry process environments. *J. Nucl. Mater.* 468, 84–96. <https://doi.org/10.1016/j.jnucmat.2015.11.010>.
- Martin Marietta Magnesia Specialties, 2016. Versamag Mg(OH)₂ MSDS. Fed. Regist. 77, 1–7.
- Meakin, P., 1988. Fractal aggregates. *Adv. Colloid Interface Sci.* 28, 249–331.
- Michaels, A., Bolger, J., 1962. Settling rates and sediment volumes of flocculated kaolin suspensions. *I&EC Fundam.* 1, 24–33.
- Nasser, M.S., James, A.E., 2009. The effect of electrolyte concentration and pH on the flocculation and rheological behaviour of kaolinite suspensions. *J. Eng. Sci. Technol.* 4, 430–446.
- Nasser, M.S., James, A.E., 2006. The effect of polyacrylamide charge density and molecular weight on the flocculation and sedimentation behaviour of kaolinite suspensions. *Sep. Purif. Technol.* 52, 241–252. <https://doi.org/10.1016/j.seppur.2006.04.005>.
- Paul, N., Biggs, S., Shiels, J., Hammond, R.B., Edmondson, M., Maxwell, L., Harbottle, D., Hunter, T.N., 2017. Influence of shape and surface charge on the sedimentation of spheroidal, cubic and rectangular cuboid particles. *Powder Technol.* 322, 75–83. <https://doi.org/10.1016/j.powtec.2017.09.002>.
- Pelssers, E.G.M., Cohen Stuart, M.A., Fleer, G.J., 1990. Kinetics of bridging flocculation role of relaxations in the polymer layer. *J. Chem. Soc. Faraday Trans* 86, 1355–1361.
- Raj, P., Batchelor, W., Blanco, A., de la Fuente, E., Negro, C., Garnier, G., 2016. Effect of polyelectrolyte morphology and adsorption on the mechanism of nanocellulose flocculation. *J. Colloid Interface Sci.* 481, 158–167. <https://doi.org/10.1016/j.jcis.2016.07.048>.
- Raj, P., Blanco, A., de la Fuente, E., Batchelor, W., Negro, C., Garnier, G., 2017. Microfibrillated cellulose as a model for soft colloid flocculation with polyelectrolytes. *Colloids Surfaces A Physicochem. Eng. Asp.* 516, 325–335. <https://doi.org/10.1016/j.colsurfa.2016.12.055>.
- Rhodes, M., 2008. Introduction to Particle Technology : Martin J. Rhodes. Wiley.
- Richardson, J.F., Zaki, W.N., 1954. Sedimentation and Fluidisation: Part I. *Trans. Instn. Chem. Engrs.* 32, 35–53. [https://doi.org/10.1016/S0263-8762\(97\)80006-8](https://doi.org/10.1016/S0263-8762(97)80006-8).
- Sharma, S. Lin, C., Miller, J. D., 2017. Multi-scale features including water content of polymer induced kaolinite floc structures. *Miner. Eng.* 101, 20–29.
- Sher, F., Malik, A., Liu, H., 2013. Industrial polymer effluent treatment by chemical coagulation and flocculation. *J. Environ. Chem. Eng.* 1, 684–689. <https://doi.org/10.1016/j.jece.2013.07.003>.
- Shi, B., Wei, Q., Wang, D., Zhu, Z., Tang, H., 2007. Coagulation of humic acid: the performance of preformed and non-preformed Al species. *Colloids Surfaces A Physicochem. Eng. Asp.* 296, 141–148. <https://doi.org/10.1016/j.colsurfa.2006.09.037>.
- Sorensen, C.M., 2001. Light scattering by fractal aggregates: a review. *Aerosol. Sci. Technol. Am. Assoc. Aerosol Res.* 35, 648–687. <https://doi.org/10.1080/02786820117868>.
- Sun, S., Weber-Shirk, M., Lion, L.W., 2016. Characterization of flocs and floc size distributions using image analysis. *Environ. Eng. Sci.* 33, 25–34. <https://doi.org/10.1089/ees.2015.0311>.
- Tang, P., Greenwood, J., Raper, J.A., 2002. A model to describe the settling behaviour of fractal aggregates. *J. Colloid Interface Sci.* 247, 210–219.
- Tomkins, M.R., Baldock, T.E., Nielsen, P., 2005. Hindered settling of sand grains. *Sedimentology* 52, 1425–1432. <https://doi.org/10.1111/j.1365-3091.2005.00750.x>.
- Ulusoy, U., Kursun, I., 2011. Comparison of different 2D image analysis measurement techniques for the shape of talc particles produced by different media milling. *Miner. Eng.* 24, 91–97. <https://doi.org/10.1016/j.mineng.2010.05.011>.
- Usher, S.P., Spehar, R., Scales, P.J., 2009. Theoretical analysis of aggregate densification: Impact on thickener performance. *Chem. Eng. J.* 151, 202–208. <https://doi.org/10.1016/j.ces.2009.02.027>.
- Vahedi, A., Gorczyca, B., 2014. Settling velocities of multifractal flocs formed in chemical coagulation process. *Water Res.* 53, 322–328.
- Vahedi, A., Gorczyca, B., 2012. Predicting the settling velocity of flocs formed in water treatment using multiple fractal dimensions. *Water Res.* 46, 4188–4194. <https://doi.org/10.1016/j.watres.2012.04.031>.
- Vahedi, A., Gorczyca, B., 2011. Application of fractal dimensions to study the structure of flocs formed in lime softening process. *Water Res.* 45, 545–556. <https://doi.org/10.1016/j.watres.2010.09.014>.
- Vajihinejad, V., Soares, J.B.P., 2018. Monitoring polymer flocculation in oil sands tailings: a population balance model approach. *Chem. Eng. J.* 346, 447–457. <https://doi.org/10.1016/j.ces.2018.04.039>.
- van Deventer, B.B.G., Usher, S.P., Kumar, A., Rudman, M., Scales, P.J., 2011. Aggregate densification and batch settling. *Chem. Eng. J.* 171, 141–151. <https://doi.org/10.1016/j.ces.2011.03.075>.
- Winterwerp, J.C., 1998. A simple model for turbulence induced flocculation of cohesive sediment. *J. Hydraul. Res.* 36, 309–326. <https://doi.org/10.1080/00221689809498621>.
- Wu, M.-Y., Adachi, Y., 2016. Effects of electrolyte concentration and pH on the sedimentation rate of coagulated suspension of sodium montmorillonite. *Appl. Colloids Surfaces A Physicochem. Eng. Asp.* 506, 686–693. <https://doi.org/10.1016/j.colsurfa.2016.07.027>.
- Xiao, F., Lam, K.M., Li, X., 2013. Investigation and visualization of internal flow through particle aggregates and microbial flocs using particle image velocimetry. *J. Colloid Interface Sci.* 397, 163–168. <https://doi.org/10.1016/j.jcis.2013.01.053>.

- Yan, Y.D., Glover, S.M., Jameson, G.J., Biggs, S., 2004. The flocculation efficiency of polydisperse polymer flocculants. *Int. J. Miner. Process.* 73, 161–175. [https://doi.org/10.1016/S0301-7516\(03\)00071-1](https://doi.org/10.1016/S0301-7516(03)00071-1).
- Zbik, M.S., Smart, R.S.C., Morris, G.E., 2008. Kaolinite flocculation structure. *J. Colloid Interface Sci.* 328, 73–80. <https://doi.org/10.1016/j.jcis.2008.08.063>.
- Zhang, D.-W., Wang, D., Liu, Z., Xie, F., 2018. Rheology, agglomerate structure, and particle shape of fresh geopolymers pastes with different NaOH activators content. *Constr. Build. Mater.* 187, 674–680. <https://doi.org/10.1016/j.conbuildmat.2018.07.205>.
- Zhang, Y., Kong, X., Gao, L., Bai, Y., 2016. Characterization of the mesostructural organization of cement particles in fresh cement paste. *Constr. Build. Mater.* 124, 1038–1050. <https://doi.org/10.1016/j.conbuildmat.2016.08.143>.
- Zhang, Y., Martin, A., Grassia, P., 2013. Prediction of thickener performance with aggregate densification. *Chem. Eng. Sci.* 101, 346–358. <https://doi.org/10.1016/j.ces.2013.06.055>.
- Zhou, Y., Franks, G.V., 2006. Flocculation mechanism induced by cationic polymers investigated by light scattering. *Langmuir* 22, 6775–6786. <https://doi.org/10.1021/LA060281+>.